PNAS
www.pnas.org

Supplementary Information for

Loss of the neural-specific BAF subunit ACTL6B relieves repression of early response genes and causes recessive autism

Wendy Wenderski, Lu Wang, Andrey Krokhotin, Jessica J. Walsh, Hongjie Li, Hirotaka Shoji, Shereen Ghosh, Renee D. George, Erik L. Miller, Laura Elias, Mark A. Gillespie, Esther Y. Son, Brett T. Staahl, Seung Tae Baek, Valentina Stanley, Cynthia Moncada, Zohar Shipony, Sara B. Linker, Maria C. N. Marchetto, Fred H. Gage, Dillon Chen, Tipu Sultan, Maha S. Zaki, Jeffrey A. Ranish, Tsuyoshi Miyakawa, Liqun Luo, Robert C. Malenka, Gerald R. Crabtree, and Joseph G. Gleeson

Co-Corresponding authors; Email: jogleeson@ucsd.edu and crabtree@stanford.edu

This PDF file includes:

Other supplementary materials for this manuscript include the following:

www.pnas.org/cgi/doi/10.1073/pnas.1908238117

Supplementary Information Text

Patient summaries

2655-III:3 was born at full term by normal delivery to a healthy mother (G3P2) after an uneventful pregnancy. The child presented clinically at 1 year of age with a single seizure in the absence of fever. There had been an older brother with intellectual disability and autistic features who similarly presented with seizures at 1 year of age and died due to a car accident. There was also a healthy older brother who achieved normal milestones. The index case continued to display seizures on a monthly basis that were described as onset with tonic stiffening of the upper extremities with head turned to the left, accompanied by drooling and upward eye deviation. Metabolic screening and karyotype were normal. EEG showed diffuse epileptiform activity, and was treated with oxcarbazepine and valproate. At the age of 2 years of age the child showed severely delayed speech, with head circumference 42.5 cm (-3SD). At age 4 years 2 months, the child showed intellectual disability (IQ 68), absent speech, hyperactivity and hypertonia. Parents report that she was unable to play with peers, showed repetitive behaviors, and self-stimulatory expressions. She was able to understand single words, and utter single syllables, and showed some ability to echo words that were repeated, but showed no ability to comprehend meaning. She met DSM-IV criteria for autism, and Conners Parent Teacher evaluation showed a score of 13, supporting a diagnosis of hyperactivity. Medical examination showed weight at the 5%ile for age. There were increased reflexes and clonus was present in the lower extremities. MRI reading was consistent with cortical and central mild atrophy with hypogenesis of the corpus callosum, but the films were lost.

2703-III:3 was the product of a pregnancy complicated by maternal hypertension and excessive weight gain to a G2P2 mother. There was a history of parental consanguinity. The child presented clinically at 2 months of age with shuddering attacks that progressed to focal epileptic seizures. EEG could not be obtained, but the seizures responded to treatment with phenobarbital. There was a history of chronic constipation and reduced weight gain. There was absent speech at 7 years, and stereotypical play with toys, such as lining up toys rather than playing with them. There were no focal neurological deficits, but mild clonus and exaggerated reflexes were present. The child met DSM-IV criteria for autism spectrum disorder. Posturing and dystonic movements were apparent, especially when he became excited. Elements of hyperactivity became apparent at 3 years of age, and the child could not sit still to watch a television show. Head circumference was 44.5 cm (-2SD) at 6 months of age. Brain MRI showed cortical and central atrophy with hypogenesis of the corpus callosum. There were two younger male siblings that presented nearly identically to the older affected individual, except that seizure onset was at 3 months or 3 weeks of age.

2727-III:6 was the product of a first cousin marriage with 3 diseased older siblings and 2 healthy older siblings, all of whom had died except for one older healthy brother. The cause of death for the older 3 affected children was chronic respiratory insufficiency resulting from aspiration pneumonia related to seizures. The unaffected child died at 2 days of life due to infection. The proband presented at 7 months of age after a history of myoclonic seizures consisting of eye blinking and facial twitching at 1 week of age, and

an EEG demonstrated burst-suppression pattern and was treated with pyridoxine, prednisone and Vigabitrin, which was switched to valproate and clonazepam. The head circumference was 42 cm (-3SD) at 10 months of age. At 3 years there was global developmental delay with IQ of 57, failure to thrive with height at weight at the 5th%ile, and mild spasticity. Potty training was not completed by 5 years of age. Biochemical assessment included amino acids, acylcarnitines, organic acids, biotinidase, pyruvate and lactate, all of which were normal. Ammonia was slightly elevated, but upon repeated assessment was normal. There were clear autistic features including self-stimulatory behavior, absent language, and stereotypical play, meeting DSM-IV criteria for autism. Brain MRI showed cortical and central atrophy of the brain, with hypogenesis of the corpus callosum.

3816-III:3 was the product of a consanguineous marriage that presented at 3 years of age with global developmental delay and seizures described as myoclonic, tonic and focal that had begun at 2 months of age, treated with valproate and vigabatrin. EEG showed subcortical discharges. Head circumference was 41.5cm (-3.1SD) at 9 months of age. There was global developmental delay, failure to thrive and mild spasticity. IQ was in the range of 50 and the child met criteria for hyperactivity and autism, but became irritable on stimulant medications, so these were stopped. Brain MRI showed cortical and central atrophy, with Hypogenesis of the corpus callosum.

4504-III:2 Was the product of a first cousin marriage that presented at 4 months of age with poor eye contact and a history of myoclonic seizures at 2.5 months. EEG showed bilateral temporal epileptiform discharges. At 4 years there was evidence of autistic features, with absent speech, posturing, abnormal eye contact, and absent of peer relationships with his cousins. Head circumference as 9 months 2as 38 cm (-2SD). Examination showed mild spasticity, brisk reflexes, dystonia, poor vision and nystagmus. Metabolic testing showed mildly elevated ammonia and lactate, which normalized upon repeat testing. Organic and amino acid testing was normal. Brain MRI showed cortical and central atrophy, hypogenesis of the corpus callosum.

5039-III:1 was the eldest child of a 2nd cousin marriage. The child presented at 3 months with poor visual contact and nystagmus, which improved, and then at age 6 years presented with atonic seizures controlled with valproate. EEG showed diffuse epileptiform activity characterized by intermittent multifocal epileptiform discharges. There was global developmental delay, IQ in the range of 50-60, and evidence of hyperactivity based upon Conners evaluations, and the child showed some positive response to stimulant medication for treatment of the hyperactivity and aggressiveness. Visual testing showed evidence of macular dysfunction, but the child had no evidence of overt visual impairment. Examination showed mild spasticity and dystonia. Brain MRI showed cortical and central atrophy, with Hypogenesis of the corpus callosum.

Materials & Methods

Human subjects

Patients were enrolled and sampled according to standard local practice in approved human subjects protocols at the University of California for blood, saliva and skin biopsy sampling.

Clinical assessments
Patients were evaluated by a child neurologist and clinical geneticist for general and neurological assessment after referral from their primary care physician for concern about developmental delay and autism. Full pedigree assessment with documentation of consanguinity and notation of siblings and cousins was performed. Intellectual function was assessed by IQ score. Speech was assessed by a speech therapist fluent in the child's native language. Brief videos of each affected member were collected during the examination as part of the clinical assessment. Autism was assessed by a clinical psychologist using ADIR, ADOS and CARS, developmental milestones were assessed with the Vineland and hyperactivity was assessed with the Conners Parent/Teacher scale, all administered in the child's native language by a trained psychologist.

Whole-exome sequencing and variant analysis
Blood was acquired from informed, consenting individuals according to institutional guidelines, and DNA was extracted using established protocols. Exome and genome sequencing was performed on both the parents and two affected member(s) from each family (where available) or a single affected member for simplex families, as previously described(1), producing average 100x read depth for exome and 30x read depth for genome sequencing. All variants were prioritized by allele frequency, conservation and predicted effect on protein function, and were tested by Sanger sequencing for segregation with disease. All families were sequenced on Illumina HiSeq2500 or HiSeq4000 instruments. All variants were prioritized by allele frequency, conservation, blocks of homozygosity, and predicted effect on protein function (see Supplemental Data), and in all families the homozygous variant in *ACTL6B* (*BAF53b*) was the top candidate. Variants were confirmed by Sanger sequencing and segregated with the phenotype according to a strict fully penetrant recessive mode of inheritance. All variants were predicted to be disease-causing by the online program Mutation Taster[18], and variants were not encountered in dbGaP, ExAC, 1000 Genomes databases, genomeAD or the Greater Middle East Variome.

Human fibroblast culture and induced pluripotent stem cell (iPSC) generation
Fibroblasts were generated from unaffected and affected dermal biopsy explants and maintained in Minimum Essential Medium (MEM, ThermoFisher Scientific cat# 11095080) supplemented with 10% Fetal Bovine Serum (FBS, Gemini Cat #100-106) and 1x Penicillin-Streptomycin (Pen/Strep 5,000 U/mL, ThermoFisher Scientific cat # 15070063). Fibroblasts were reprogrammed at iGentBio (San Diego) to generate induced pluripotent stem cells (iPSCs) as previously described(2), using episomal non-integrating expression of Oct3/4, Sox2, Klf4, c-Myc by Sendai viral transduction. There were 3 clones generated per subject that were individually assessed. Lines used in these experiments were tested for: 1] Free of evidence virus. 2] G-banding and karyotyping. 3] SNP panel cell line barcode. 4] Pluripotent marker antibody staining. 5] Pluripotent gene expression profiling. 6] Embryoid body formation and gene expression profiling. 7] Contamination free from mycoplasma routinely performed monthly.

Human pluripotent cell culture
Control or patient-derived iPSCs were cultured in mTeSR1 medium (Stemcell Tech.) on plates coated with Geltrex (ThermoFisher) and passaged with Accutase (Stemcell Tech.) every 4-5 days according to published methods(3).

Differentiation and culture of human iPSC-derived neural precursor cells (NPCs) and neurons
NPCs were generated from iPSCs as described(2), plated on 6-well plates coated with poly-ornithine (PLO, 15ug/mL, Sigma P3655) and laminin (10ug/mL, Invitrogen 23017-015) and cultured in Neuronal Differentiation Medium: Dulbecco's modified Eagle's medium, Nutrient Mixture F-12 (DMEM/F12, ThermoFisher cat# 10565018) supplemented with 1x N2 (Gibco cat# 17502-048), 1x B27 (Gibco cat# 17504-044), BDNF, 20 ng/ml; Peprotech, cat# 450-02), GDNF, 20 ng/ml; Peprotech cat# 450-10), ascorbic acid (AA, 200 nM; Sigma, cat# A0278), and dibutyryl cyclic AMP, 1mM Sigma, cat# D0627). After 4 weeks differentiation, the medium was switched to BrainPhys basal medium for an additional 8 weeks before phenotyping, as described(4).

Human brain organoid culture
Patients specific iPS cells were obtained from (Burnham Stem Cell core) and at passage 4, were verified normal karyotypes, pluripotency and contamination-free. All these iPS cells lines were maintained in mTeSR as mentioned above and regulatory tested and confirmed negative for mycoplasma. On day 0 of organoid generation, iPS cells at 12 passages were dissociated with Accutase (Thermo Fisher Scientific, A1110501) to singles cells. In total, 9,000 cells were then plated in each well of an ultra-low-attachment 96-well plate (Corning, CLS3474) in Cortical differentiation medium(5) with addition of 20 µM Rock inhibitor (Y-27632, Sellek, S1049), 5µM SB431542 (R&D, 1614), 3 µM endo-IWR-1 (R&D, 3532) for the first 4 days; after which, medium was changed every two days for 13 days with the Cortical differentiation medium(5) with addition of 5 µM SB431542, 3 µM endo-IWR-1. On day 18, the immature organoids were transferred into the ultra-low-attachment 6-well plate (Corning, CLS3471) and cultured for 16 days with Organoid differentiation medium(5), with media changed every 3~4 days. On day 35, the Organoid differentiation medium was changed into Maturation medium(5) with addition of 1% Matrix High Concentration (HC), Growth factor reduced (GFR) Matrigel (Corning, 354263). Media was changed every 3~4 days for additional 34 days, with fresh HC-GFR Matrigel added at each media change. On day 70, the Maturation medium was exchanged for Long-term maintain medium(5) in addition with 2% HC-GFR-Matrigel, 50 ng/ml BDNF (R&D, 248-BD-025/CF) and 50 ng/ml GDNF (R&D, 212-GD-010/CF) for maintaining the organoids.

Immunostaining human brain organoids
Organoids were fixed in 4% paraformaldehyde for 15 min at room temperature followed by washing with PBST (PBS with 0.25% Tween20) 3x 5 min. Fixed organoids were then allowed to sink in 30% sucrose overnight at 4 ºC, and embedded in 15%/15% gelatin/sucrose solution and cryosectioned at 20 mm. Organoid sections were permeabilized in 0.25% Triton X-100 for 15 min at room temperature and blocked with

10% BSA in PBS for 1h at room temperature. After washing 3 x 5 min with PBST, sections were incubated with primary antibodies in 5% BAS in PBS overnight at 4 ºC. The next day, organoids were washed with PBST 3 x 10min, before incubating with secondary antibodies for 2 h at room temperature. Organoid sections were washed again 3 x 5 min with PBST and mounted with the fluorescence mounting medium (Dako, cat# S3023). Images of brain organoids were taken with ZEISS LSM880 Airyscan and analysis was done in ImageJ.

Animals

Animals used in this research included fruit flies and two separate cohorts of mice: (1) male and female wild type, *Actl6b*$^{+/-}$ and *Actl6b*$^{-/-}$ littermate mice of highly backcrossed C57BL/6 background, age 7-11 weeks, bred at Stanford University and (2) male wild type or *Actl6b*$^{-/-}$ littermate mice, age 12-16 weeks, that were the F1 offspring of *Actl6b*$^{+/-}$ 129S6/SvEV x *Actl6b*$^{+/-}$ C57BL/6 bred at Fujita Health University. At Stanford, wild type, *Actl6b*$^{+/-}$ and *Actl6b*$^{-/-}$ male or female mouse(6) littermates were housed up to 5/cage in a colony with a 12-hour light/dark cycle (lights on from 7:00 A.M. to 7:00 P.M.) at constant temperature (23 ºC) with ad libitum access to water and food. Although *Actl6b*$^{-/-}$ were originally reported to not survive weaning on the 129S6/129/SvJ mixed background, we backcrossed the line to C57BL/6J for >10 generations and recovered Mendelian ratios of the expected genotypes at weaning. For primary mouse neuronal culture experiments, embryonic cortical neurons were harvested from E16.5 or E18.5 *Actl6b*$^{+/-}$ x *Actl6b*$^{+/-}$ littermates from pregnant female mice. Flies were raised at 25 °C on standard cornmeal-molasses media. Animal protocols were approved by IACUC at Stanford University. The second cohort of *Actl6b* null mice was group-housed (three or four animals per cage) in a room with a 12-h-light, 12-h-dark cycle (lights on at 7:00) and with access to food and water ad libitum. Behavior tests were performed with male mice at 12–50 weeks of age between 9:00 and 18:00 unless otherwise stated. Mouse care and all behavior experiments were approved by the animal ethics committee of Fujita Health University.

Mouse Behaviors

Juvenile Interaction**:** The juvenile interaction was performed in the home cage of the test animal as previously described(7). *Actl6b* mouse cagemates (age 7-11 weeks, C57BL/6 cohort) were temporarily moved to a holding container and the test mouse was habituated for 1 min. Following habituation, a novel conspecific juvenile mouse (same gender, 3-5 weeks) was placed into the home cage for 2 min of free interaction. All sessions were video recorded with a camera located above the home cage and analyzed manually followed the behavior. Interaction time was limited to when the test mouse was exploring the juvenile mouse as defined by active pursuit, sniffing any region including the snout, body, anogenital area, and grooming. These parameters were not assayed independently. All behavior was scored blindly to the genotype of the mice.

Adult Interaction: The adult social-interaction test was performed as described previously(8). Briefly, two 13–17 week old male mice of the same genotype that were strangers to each other were placed together in a box (40 × 40 × 30 cm) and allowed to explore freely for 10 min. The total duration of contact was measured automatically by ImageSI software.

3-chamber**:** A 3-chamber sociability assay was performed in an arena with three separate chambers as previously described(9). On day one, the test mice (age 7 – 11 weeks, C57BL/6 cohort) were habituated to the arena, with two empty wire mesh cups (with tops covered to prevent mice from crawling on top) placed in the two outer chambers for 5 min. The juvenile mice were also habituated to the mesh cups for 5 min following test mice habituation. On day two, the test mouse was placed in the center chamber and a conspecific juvenile (same gender, 3-5 weeks) was placed into one of the wire mesh cups. The test mouse was placed in the center chamber for 2 min. The barriers were raised and the test mouse was allowed to explore freely for a 20 min session. The placement of juvenile mice in the chamber was also counterbalanced across session. Location of mice was assayed automatically using a video tracking system (BIOBSERVE). Sociability was calculated as ([time in juvenile side – time in empty side]/[time in juvenile side + time in empty side]).

Novel Object**:** The novel object assay was performed in an identical manner to the juvenile interaction assay, where a novel toy mouse instead of a live mouse was placed into the animal's home cage. Investigation time was again 2 min.

Open Field Test**:** To assay the effects of genotype on locomotor activity and anxiety, an open field test was conducted according to standard methods (10, 11). Two cohorts of mice were assayed: (1) male and female wild type, *Actl6b*$^{+/-}$ and *Actl6b*$^{-/-}$ littermate mice of highly backcrossed C57BL/6 background, age 7-11 weeks, bred at Stanford University and (2) male wild type or *Actl6b*$^{-/-}$ littermate mice, age 12-16 weeks, that were the F1 offspring of *Actl6b*$^{+/-}$ 129S6/SvEV x *Actl6b*$^{+/-}$ C57BL/6 bred at Fujita Health University. For both cohorts, the test mouse was placed in an open field area (40 cm x 40 cm) with center zone defined 20 cm x 20 cm. Mice were allowed to move freely for a 20 min session and the total distance travelled and time in center zone were assayed automatically using a video tracking system (BIOBSERVE). In addition, the Fujita Health University cohort was assayed in the open field for 120 minutes and analysis also included measurement of repeated breaks of the same photobeam, or "stereotypic counts" (Accuscan Instruments).

T-maze Forced Alternation Test: To assay the effects of genotype on working memory, wild type or *Actl6b*$^{-/-}$ male F1 offspring of a *Actl6b*$^{+/-}$ 129S6/SvEV x *Actl6b*$^{+/-}$ C57BL/6 cross, age 42-47 weeks, were assayed in a T-maze forced alternation test as described previously(8). Briefly, mice were pretrained by "forcing" movement (through the opening of doors) towards one arm of a T maze to receive a food reward. After consuming the reward, the test mouse was ushered back to the start of the T and given free choice between the two arms of the T maze. Choice of the opposite arm to where it was first rewarded resulted in a new food reward. An "incorrect choice" occurred if the mouse chose the same arm where it last received a treat. On days 6-8 of repeated testing in this manner, mice were challenged with 3, 10, 30, and 60 s delays between the forced choice and free choice trials of each pair. Data acquisition and analysis were performed automatically with ImageTM software.

Barnes Maze Test: To assay the effects of genotype on spatial memory, wild type or *Actl6b*$^{-/-}$ male F1 offspring of a *Actl6b*$^{+/-}$ 129S6/SvEV x *Actl6b*$^{+/-}$ C57BL/6 cross, age 17-21 weeks, were assayed in a Barnes maze test as described previously(8). Briefly, a white, circular open field of 1 m diameter with 12 holes was elevated 75 cm from the floor. Connected to one holes was a black Plexiglas "target" escape box (17 × 13 × 7 cm)

containing paper cage-bedding on its floor. Distal cues were available to orient the mouse to the location of the "target" escape route. Individual mice were trained on a specific hole each day and the latency to reach the target hole, number of errors, and the time spent around each hole were recorded with the use of ImageBM software.

Immunostaining mouse brain

Adult mice were deeply anaesthetized by intraperitoneal injection of 40-50 mg/kg of sodium pentobarbital and euthanized by transcardial perfusion with ice cold phosphate buffered saline (PBS) pH 7.4 and then 4% paraformaldehyde in PBS. Whole mouse brains were postfixed in 4% paraformaldehyde/PBS for 48 hours at 4 °C and then washed 3x with PBS. Brains were sliced coronally on a vibratome to 50 μm thickness and stored at 4 °C in PBS supplemented with 0.02% sodium azide. Single brain slices were placed individual wells of a 24 well plate and blocked & permeabilized with 150 μL of 5% normal donkey serum/0.3% Triton X-100 in PBS for 1 h at room temperature, with gentle agitation. Afterwards, 50 μL containing 4x final concentration of primary antibodies in 5% normal donkey serum/0.3% Triton X-100/PBS was aliquoted into each test well, giving a total volume of 200 μL with 1x antibody concentrations. Slices were incubated at 4 °C overnight in a humidity chamber, with very slow and low-incline rocking. Primary antibody solutions were completely removed and slices were washed 3x 5 minutes with agitation at room temperature with 400 μL 0.1% Tween-20 in PBS. Secondary antibodies were then applied for 1 h in 5% normal donkey serum/0.3% Triton X-100/PBS with gentle agitation at room temperature, followed by washing as before. Using a paintbrush, slices were placed into a drop of water and positioned on a Superfrost microscope slide (FisherSci). Water was carefully aspirated and a drop of ProLong Diamond Antifade Mountant with DAPI (Thermo Fisher Scientific cat# P36971) was placed on each brain slice, followed by a coverslip. Slices were imaged the next day.

Mouse brain imaging and callosal analysis

Mouse brain slices from different animals were imaged in an automated fashion under exactly the same capture conditions using on a Keyence BZ-X700 system. This involved first finding the maximum intensity setting for each channel across all genotypes and locking in these capture conditions. Then, the position of each brain to be imaged was programmed in and the BZ-X700 robotically imaged each brain in the 3 slide holder (usually 2 wild type, 2 heterozygotes and 2 knockouts) under the programmed conditions, saving each as a separate file. All brain images for a given condition were processed using identical haze reduction and black balance conditions. For analysis, matching male or female sets of wild type, heterozygous and homozygous knockout brain slices were identified. Images were de-identified and measurements (arbitrary units) were taken using ImageJ for cortical and corpus callosum thickness. Note that staining with myelin basic protein (MBP) or neurofilament light chain (NFL) gave nearly identical thickness ratios for KO/WT or het/WT and thus, these values were averaged for each individual and plotted as bar graphs.

Primary neuron culture

Embryonic day 16.5 (E16.5) or 18.5 (E18.5) primary mouse cortical neurons were used in this study. Pregnant female mice were anesthetized with isoflurane and euthanized by

cervical dislocation on E16.5 or E18.5. Cortical or striatal neurons were cultured following a protocol described by Maze and colleagues (12). Specifically, culture plates (Corning, cat# 353003) were coated overnight at 37 °C with poly-D-lysine (0.1 mg/mL, Sigma, cat# P6407) in borate buffer. Plates were washed 3x with water or PBS prior to plating neurons. Embryonic cortices or striatum were harvested and enzymatically dissociated to single neurons with the Neural Tissue Dissociation Kit (P) (Miltenyi Biotec, cat# 130-092-628). Cortical neurons from separate pups were resuspended in plating media [DMEM (Life Technologies cat#11960-077) containing 10% FBS (Omega cat#FB-01) and 1x penicillin-streptomycin (ThermoFisher cat#15140122)], counted with a Hemocytometer and plated at a density of approximately one brain (~ 5.5 x10^6 neurons) per 6-well or 10 cm plate. Striatal or hippocampal neurons were plated at the same density (~9 x10^5 neurons per well of a 6-well plate). Following undisturbed incubation for 1 hour at 37 °C, neurons attached to the plates and the media was exchanged with maintenance media [Neurobasal Medium (Life Technologies, cat# 21103049) supplemented with 2.5% B27 (Thermo Fisher, cat# 17504044), 1% penicillin-streptomycin (Life Technologies cat# 15070-063), 0.25% GlutaMAX (Life Technologies, cat# 35050061)]. On day in vitro (DIV) 2, ARA-C (Sigma, cat# C1768) was added to a final concentration of 0.5 μM. Beginning on DIV 3, one-half of the media was exchanged for fresh media every three days. Neurons were stimulated and collected on DIV 7. For ACTL6B rescue experiments, neurons were infected on DIV 4 and induced with 1 μg/mL doxycycline continuously for 2 weeks beginning on DIV 6.

KCl stimulation

Neurons were depolarized on DIV 7 with 50 mM KCl for 1 or 6 hours as described(12-14), then collected in TRIzol or flash-frozen and stored at -80 °C. The excitotoxicity-induced gene *Clca1* was verified not to be upregulated (see **Dataset S1**), excluding toxic reaction.

Cloning and generation of human *ACTL6B* mutants

Wild type human *ACTL6B* was subcloned into pDONR and then into pINDUCER20 vector(15) using the Gateway method (ThermoFisher). Point mutations were introduced into pDONR-*ACTL6B* using the QuikChange Site-Directed Mutagenesis Kit (Stratgene).

Lentivirus production and transduction

Lentivirus were produced from approximately 18 million Lenti-X 293T cells (Clontech, cat# 632180) via polyethylenimine transfection. Media from first 24 h post-transfection was discarded and replaced with 30 mL media. After 48 h, viral media collected and centrifuged for 2 h at 20,000 RPM. Viral pellets were resuspended in 250 μL PBS. Relative titer for wild type or mutant ACTL6B-containing viruses was estimated from infection of HEK293Ts with viral media and selection with 500 μg/mL G418 (ThermoFisher cat# 10131035). HEK293Ts were infected with 1 mL viral media per well of a 6-well plate. Between 10-20 uL concentrated virus was applied per well of a 6-well plate containing primary neurons or hESCs. Virus was applied with 10 μg/ml Polybrene (Santa Cruz, cat# sc-134220) to hESCs only. HEK293Ts and hESCs were continuously selected with 500 μg/mL G418. For A representative well for each pINDUCER20-

ACTL6B construct was selected with 500 μg/mL G418 to confirm high transduction efficiency.

Preparation of neuronal, hESC or HEK293T nuclear extracts.
Neurons were collected by cell lifter on ice in PBS, while H9 hESC or HEK293T cells were collected by detachment with Accutase (Thermo Fisher, cat# A11105-01) or 0.25% trypsin (Life Technologies, cat# 25200056), respectively, followed by quenching with serum-containing media. Cells were counted using a hemocytometer and divided into $2x10^7$ cell aliquots, then resuspended in 1 mL of ice cold Buffer A [10 mM HEPES, pH 7.5, 25 mM KCl, 1 mM EDTA, 0.1% NonidetP-40, 10% glycerol, plus 1 mM DTT, protease inhibitor tablet (Roche), 1 mM sodium orthovanadate, and 10 mM sodium butyrate freshly added at time of use] to release nuclei. The volume of Buffer A was brought up to 10 mL and the cells were incubated on ice for 5 minutes to ensure lysis. Nuclei were pelleted by centrifugation at 1500 RPM for 5 min at 4 °C. Nuclei were gently resuspended and washed with 10 mL Buffer A, centrifuged, and then nuclei resuspended with Buffer C [10 mM HEPES pH 7.5, 100 mM KCl, 1 mM EDTA, 3 mM MgCl2, 10% glycerol plus 1 mM DTT, protease inhibitor tablet (Roche), 1 mM sodium orthovanadate, and 10 mM sodium butyrate freshly added at time of use] at 0.6 mL per $2x10^7$ cells. To selectively precipitate DNA, a 1:10 vol of 3 M ammonium sulfate was added drop-wise and samples were rotated at 4 °C for 30 min. DNA was pelleted by ultracentrifugation at 100,000 RPM for 15 min at 4 °C. The supernatant was transferred to a fresh tube and ammonium sulfate powder was added at 0.3 g/mL to precipitate soluble nuclear proteins. Nuclear proteins were precipitated for 20 min on ice and then centrifuged at 100,000 RPM for 15 min. The protein pellet containing nuclear proteins was stored in -80 °C.

Preparation of brain nuclear extracts for affinity purification
For routine affinity purification, freshly dissected P0 mouse brains were rinsed in cold HBSS then to 10 mL ice Buffer A. Nuclei were released from brain tissue by douncing with ten strokes of the loose-fitting size glass Dounce homogenizer, followed by 10 strokes with the tight-fitting Dounce. Nuclei were pelleted by centrifugation at 1700 x g for 10 minutes, washed 2x 5 mL Buffer A and 1x with 3 mL Buffer C. DNA and soluble nuclear proteins were fractionated using the ammonium sulfate precipitation method described above. For the μLC-MS/MS study, fresh E18.5 mouse cortices were dissociated to single cells using the Neural Tissue Dissociation Kit (P) (Miltenyi Biotec, cat# 130-092-628) and depleted for glia using the Anti-Prominin-1 MicroBead Kit (Miltenyi Biotec, cat# 130-092-333). Neurons were counted with a hemocytometer and nuclear extract was prepared as above.

Antibodies for affinity purification and Western blot
nBAF complexes were immunopurified for mass spectrometry using with α-SMARCA4 (H-10 Santa Cruz, cat# sc-374197 or G-7 Santa Cruz, cat# sc-17796) antibodies. nBAF complexes from P0 brain were purified with an α-SS18L1 (CREST) (M-15 Santa Cruz, cat# sc-50912) antibody. For Western blotting, the above antibodies were used and additionally: homemade antibodies α-BAF170(16), α-BAF155(17), α-ACTL6A and α-ACTL6B(6, 16, 18); and commercially available antibodies α-SMARCA4 (H-88) (Santa

Cruz, cat# sc-10768), α-TOP2B (F-12) (Santa Cruz, cat# sc-365916), α-INI1/BAF47 (A-5) (Santa Cruz, cat# sc-166165), α-ACTL6A (Novus, cat# NB100-61628), α-total BAF53 (Cell Signaling cat# 43910), α-GAPDH (6C5) (Santa Cruz, cat# sc-32233), α-MOZ/KAT6A (4D8) (Santa Cruz, cat# sc-293283), α-MYH9 (H-40) (Santa Cruz, cat# sc-98978). Goat or donkey, α-mouse or α-rabbit IRDye 800CW or 680LT (LI-COR) secondary antibodies were used for Western blot analysis with an Odyssey CLX imaging system (LI-COR).

Antibodies for immunostaining mouse and human tissues

For mouse immunostaining experiments, primary and secondary antibodies were diluted to the final concentrations specified below in 5% normal donkey serum/0.3% Triton X-100 in PBS. Primary antibodies included: α-neurofilament light chain (NFL, clone C28E10) (Cell Signaling cat# 2837) diluted 1:200, α-myelin basic protein (MBP) (Cell Signaling cat# 78896) diluted 1:300. Secondary antibodies were all diluted 1:200 and included: donkey α-mouse Alexa Fluor 488 (Invitrogen cat# A-21202), donkey α-rabbit Alexa Fluor 555 (Thermo Fisher Scientific cat# A32794), donkey α-goat Alexa Fluor 647 (Thermo Fisher Scientific cat# A32849). For immunostaining human brain organoids, the following dilutions and primary antibodies were used: SOX2 (Santa Cruz Biotechnology, cat# sc17319) at 1:100, TUJ1 (Biolegend cat# 801202) at 1:1000, ACTL6A (Novus Biologicals, NB100-61628) at 1:500, ACTL6B (home-made by Crabtree Lab in Stanford)(6) at 1:500.

Antibody crosslinking

For all affinity purifications except that used for the mass spectrometry study, antibodies were first crosslinked to beads using BS^3 (ThermoFisher, cat# 21580). For each sample, 3-8 μg antibody was pre-bound to 50 μL Protein G Dynabeads (ThermoFisher, cat# 10004D) slurry in 500 μL 1xPBS (ThermoFisher, cat# 10010049) for at least 15 minutes. The beads were washed 2x with 1 mL 1xPBS and then 2x in 200 μL BS^3 conjugation buffer (20 mM sodium phosphate, pH 7, 150 mM NaCl). 250 μL of freshly prepared 5 mM BS^3 crosslinking reagent in conjugation buffer was added to each 50 μL bead sample and rotated at room temperature for precisely 15 minutes. At the 15 min point, 6.25 μL 2 M Tris, pH 8, was added to each tube to quench the crosslinking reaction. The beads were then washed 3x in IP buffer and used immediately. For mass spectrometry, homemade J1B α-SMARCA4/SMARCA2 or α-rabbit antibodies were crosslinked to Fast-Flow Protein A Sepharose beads (GE, cat# 17-5280-01) using dithio-bis(succinimidyl propionate) (DSP, Pierce, cat# 22585) following a published protocol(16).

Affinity purification of nBAF complexes

Ammonium sulfate precipitated nuclear extracts were resuspended on ice in immunoprecipitation (IP) buffer. For all immunoprecipitation experiments except that used for mass spectrometry, the IP buffer consisted of 20 mM HEPES, pH 7.4, 150 mM KCl, 1 mM EDTA, 1 mM MgCl2, 0.1% Triton X-100, 10% glycerol, freshly supplemented with protease inhibitors (complete, Roche, cat# 11836153001), 1 mM DTT, 10 mM sodium butyrate (Sigma, cat# 303410), 1 mM sodium orthovanadate (Calbiochem, cat# 567540). BAF complexes were immunoprecipitated overnight at 4 °C

with BS^3-crosslinked α-SMARCA4 mouse antibody (Santa Cruz, SMARCA4 clone G-7 or H-10) on Protein G Dynabeads (ThermoFisher, cat# 10004D). The next day, supernatant ("flow-through") was removed and saved for depletion analysis, and the protein-bound beads were washed 5x with 250 mM KCl immunoprecipitation buffer. BAF complexes were eluted by boiling with 40 µL 1.1x LDS Sample Buffer (Life Technologies, cat# NP0007). For mass spectrometry, neuronal nuclear extracts were pre-cleared for 30 minutes at 4 °C with α-rabbit crosslinked Fast-Flow Protein A Sepharose beads (GE, cat# 17-5280-01) in binding buffer [300 mM NaCl, 50 mM Tris-HCl (pH 8.0), 1% NonidetP-40, 0.5% deoxycholate, 0.1% SDS, supplemented with protease inhibitors]. nBAF complexes were bound to beads by rotating overnight at 4 °C with J1B α-SMARCA4/SMARCA2 antibody crosslinked to Fast-Flow Protein A Sepharose beads (GE). Bound complexes were washed three times for 10 minutes in 300 mM NaCl, 50 mM Tris-HCl (pH 8.0), 1% NonidetP-40, 0.5% deoxycholate, 0.1% SDS, twice in 0.1 M KCl, 20 mM HEPES (pH 7.9), 10% glycerol and 0.1 mM EDTA and once in distilled water. Purified complexes were eluted in 0.1 M glycine pH 2.5 and neutralized immediately in 1/10 vol. of 1 M Tris-HCl (pH 8.3).

Mass spectrometry (µLC-MS/MS)

Eluted nBAF protein complexes (n=1 of each genotype, pooled from multiple individuals) were denatured with 6M Urea, reduced with 5mM dithiothreitol, alkylated with 25mM iodoacetamide, and digested with Lys-C for 3 h (1:200 w:w, 37C; Promega) followed by Trypsin overnight (1:25 w:w, 37C; Promega). Peptides were acidified with formic acid and purified using C18 reversed-phase chromatography (Nest Group). Peptides from wild type or *Actl6b*$^{-/-}$ nBAF complexes were isotopically labeled with light (d0) and heavy (d4) mTRAQ reagents (Sciex), respectively, according to manufacturers' protocol. Labeled peptides were subsequently combined, and separated into 9 fractions with strong cation exchange (PartiSphere SCX; Hichrom) resin using in house packed microbore guard columns (Upchurch Scientific) and a syringe pump (30µl/min; Harvard Apparatus). Peptides were eluted with a stepwise gradient of 25mM, 40mM, 50mM, 60mM, 75mM, 100mM, and 750mM NH4-Formate in 5% Acetonitrile (19). Eluted peptide fractions were evaporated, and then separated by HPLC (Eksigent nanoLC Ultra) with C18-reversed phase columns packed 2cm (trap) and 15cm (analytical) in house (ReproSil-Pur C18-AQ 3um; Dr. Maisch) over an increasing gradient of 2-35% Buffer B (100% acetonitrile, 0.1% formic acid) over 100min at a flow rate of 280nL/min. Eluted peptides from each of 9 fractions were analyzed with an LTQ Orbitrap Velos mass spectrometer (Thermo Fisher Scientific) operated in data dependent mode, with the Top5 most intense peptides per MS1 survey scan selected for MS2 fragmentation by collision-induced dissociation (CID). MS1 survey scans were performed in the Orbitrap at a resolution of 30,000 at m/z 400 with charge state rejection enabled, while CID MS2 was performed in the dual linear ion trap with a minimum signal of 500. Lock mass calibration to ambient air was performed (429.088735, 445.120025). Dynamic exclusion was set to 30 s. Raw output data files were searched against the IPI murine database (v3.69) using X!Tandem (Thermo Scientific) to identify peptides. Probabilities were determined by PeptideProphet, iProphet, and ProteinProphet(20-22), and quantification was performed by ASAP Ratio (23), as part of the Trans-Proteomic Pipeline. Data was manually inspected to ensure accuracy of identifications and quantifications.

Salt fractionation of chromatin binding proteins
Nuclei were prepared using cold Buffer A as in "Preparation of neuronal, hESC or HEK293T nuclear extracts". Five standard salt concentrations (300, 400, 500, 600, 700 mM NaCl)(24) were prepared in TE buffer. Salt solutions were added to pure nuclei at a ratio of about 50 µL per 2 million cells and incubated on ice for 10 minutes, flicking halfway through to resuspend. Following a 10 minute spin at 800xg, the supernatant ("soluble nuclear" fraction) was separated to a new tube and the remaining pellet was solubilized in sample buffer with sonication for 15 minutes using a Bioeruptor (Diagenode) set to high with 30 s ON/30 s OFF cycles.

Western blotting
The concentrations of nuclear or cytoplasmic proteins (see nuclear extract preparations above) were determined by Bradford Assay (Bio-Rad, cat# 5000006) and diluted to either 0.5 µg/mL or 1 µg/mL in LDS Sample Buffer (Life Technologies, cat# NP0007). Whole cell extracts were prepared by diluting exactly $1x10^6$ cells in 100 µL 1.5x LDS Sample Buffer and sonicating on high 30 s ON/30 s OFF for 10 minutes in a Bioeruptor (Diagenode). 1 µL concentrated β-mercaptoethanol (14.3 M) was added per 100 µL of lysate and the samples were boiled for 5 minutes to fully denature and reduce proteins. 10 µL of whole cell extract or 3-7 µg ammonium sulfate precipitated nuclear extract or 10-20 µg cytoplasmic extract was loaded into a 4–12% BisTris NuPage gel (ThermoFisher, cat# np0321box). Proteins were transferred at overnight at 4 °C overnight at 85 mA to PVDF membranes (ThermoFisher, cat# ipvh000-10). Membranes were blocked in 5% BSA/TBST. Blots were then incubated with primary antibodies for 2 h at room temperature (or overnight at 4 °C) and for 1 h at room temperature with secondary antibody. Proteins were detected with an Odyssey CLX imaging system (LI-COR) detection system.

Protein structure prediction
The "Hetero Project" feature of web-based protein structural modeling resource, SWISS-MODEL(25-31), was used to generate heterotypic models of wild type or mutant human *ACTL6B/*BAF53B isoform 1 with the SMARCA4-HSA domain and β-actin (actin not shown in model for clarity). Briefly, SWISS-MODEL performed a homology search for structural templates using NCBI-BLAST and HHBlits. The protein structural template alignment was performed using ProMod3 and conserved coordinates were used to build the primary model of ACTL6B with SMARCA4-HSA and β-actin. A fragment library was employed to model regions that were not well conserved. The model of human ACTL6B/SMARCA4-HSA/β-actin reported here was constructed primarily based upon homology to *S. cerevisiae* Arp4 and its crystal structure in ternary complex with actin and the HSA domain of the SWI/SNF ATPase Swr1(32).

***In silico* prediction of ACTL6B mutant protein stability**
The 3D structure of ACTL6B was created using SWISS-MODEL (see above). This initial structure was subjected to relaxation using Discrete Molecular Dynamics (DMD)(33) simulation to remove interatomic clashes. The simulation was run for 10,000 steps at temperature T=0.5 kcal/(mol k_B) with a high value of heat exchange coefficient

C=10 to make sure that excess of potential energy due to interatomic clashes would dissipate with minimal perturbations to initial structure. The resulting relaxed ACTL6B structure was used for ΔΔG calculations performed with standalone Eris software package(34). Eris was employed using fixed backbone setting. For each mutation, ΔΔG was calculated as average over 30 individual Eris runs with different initial seed values.
PolyPhen-2(35), MuPRO(36) and iMutant 2.0(37) were used as secondary methods to predict the effect of human ASD *ACTL6B* mutations on protein stability. Only PolyPhen-2 scores were reported in Figure 1.

	PolyPhen-2							
	HumDIV			HumVar			MuPRO	iMutant 2.0
BAF53b mutant	Score (0-1, 1= damaging)	Sensitivity	Specificity	Score (0-1, 1= damaging)	Sensitivity	Specificity	Effect on stability	Effect on stability
L154F	0.999	0.14	0.99	0.989	0.52	0.95	Decrease	Decrease
T175P	0.99	0.72	0.97	0.91	0.69	0.9	Decrease	Decrease
G393R	1	0	1	1	0	1	Decrease	Decrease
G417W	1	0	1	1	0	1	Decrease	Decrease

MARCM analysis

Heat-shock-flp (hsFlp) based MARCM analyses were performed as previously described(38, 39). Briefly, transgenic flies linked with a FRT chromosome (e.g., *FRTG13, Bap55*$^{-}$ and *FRTG13, Bap55*$^{-}$*; UAS-ACTL6B*^{WT}) were crossed with MARCM-ready flies (containing hsFlp, UAS-CD8GFP, GH146-GAL4(40), TubP-GAL80 and desired FRT). Larvae (0 h to 24 h after hatching) from the cross were heat shocked for 1h in a 37°C water bath. Both single-cell and neuroblast clones could be observed in this fashion. Confocal images were collected with a Zeiss LSM 780 and processed with ImageJ and Adobe Illustrator.

Fly genotypes:

UAS-mCD8GFP, hsFLP; FRTG13, TubGAL80; GH146-GAL4

UAS-mCD8GFP, hsFLP; FRTG13, TubGAL80/FRTG13; GH146-GAL4

UAS-mCD8GFP, hsFLP; FRTG13, TubGAL80 /FRTG13, Bap55^{-}*; GH146-GAL4*

UAS-mCD8GFP, hsFLP; FRTG13, TubGAL80 /FRTG13, Bap55^{-}*; UAS-ACTL6B*^{WT}*; GH146-GAL4*

UAS-mCD8GFP, hsFLP; FRTG13, TubGAL80 /FRTG13, Bap55^{-}*; UAS-ACTL6B*^{154}*; GH146-GAL4*

UAS-mCD8GFP, hsFLP; FRTG13, TubGAL80 /FRTG13, Bap55^{-}*; UAS-ACTL6B*^{393}*; GH146-GAL4*

Immunostaining fly brain

Fly brains were dissected in 1x PBS and then fixed in 4% paraformaldehyde. Immunostaining was performed following previously described methods(41). Primary antibodies used in this study include rat α-DNcad (DN-Ex #8; 1:40; DSHB) and chicken α-GFP (1:1000; Aves Labs, cat# GFP-1020). Secondary antibodies were from Jackson Immunoresearch, conjugated to Alexa 488 or Alexa 647.

RNA Isolation and Quantitative Polymerase Chain Reaction (qPCR)

For reverse-transcriptase quantitative PCR (RT-qPCR), total RNA was isolated using TRIzol (Life Technologies). One microgram of RNA was reverse transcribed using the High-Capacity cDNA Reverse Transcription Kit (Applied Biosystems, cat# 4368814). Samples were prepared using the SensiFAST SYBR Lo-Rox kit (Bioline, cat# BIO-

94020), according to the manufacturer's instructions. Analysis of qPCR samples was performed on a QuantStudio 6 Flex system (Life Technologies). At least two technical and three biological replicates were used for each condition. The ΔΔCt method was used to determine transcript abundance relative to glyceraldehyde-3-phosphate dehydrogenase (*Gapdh*). Statistical significance for differences between the 3 *Actl6b* genotypes was calculated using one-way ANOVA with Tukey's correction for multiple comparisons, or if only 2 genotypes or conditions were compared, a Student's t-test was used (GraphPad).

RNA-seq Library Preparation

Neurons were washed 1x with ice-cold PBS and collected with 1 mL per 6-well TRIzol (Life Technologies, cat# 15596081). Total RNA was extracted and DNAse treated using the DirectZol kit (Zymo Research cat# R2060). RNA quality was confirmed by Bioanalyzer (Agilent). Individual RNA libraries were prepared with unique barcodes using the SMARTer Stranded Total RNA Sample Prep HI Kit (Clontech cat# 634874). Libraries were quantified by PCR using a PhiX library (Illumina cat# TG-110-3001) standard curve and then multiplexed at a 1:1 ratio. Pooled libraries were run on the NextSeq 500 (High 2x75 bp) (Illumina) at the Stanford Functional Genomics Facility.

ATAC-seq Library Preparation

Neurons were washed and collected in ice-cold PBS using a cell lifter (Corning #3008), and then counted using a Countess II FL cell counter (Applied Biosystems). Accessible chromatin from 55,000 neurons per biological sample were transposed and tagged using Tn5 (Nextera DNA Sample Prep Kit from Illumina, cat# FC-121-1030), then barcoded and amplified following a published protocol (42). DNA fragment sizes were determined using a TapeStation (Agilent) with High Sensitivity D1000 Screentapes (Agilent cat# 5067-5584) and showed the expected pattern for non-nucleosomal and nucleosomal sizes. Libraries were quantified by PCR using a PhiX library (Illumina cat# TG-110-3001) standard curve and then multiplexed at a 1:1 ratio. Pooled libraries were run on the NextSeq 500 (High 2x75 bp) (Illumina) at the Stanford Functional Genomics Facility.

Analysis of RNA-seq datasets

RNA-seq reads were mapped to the mm9 mouse genome using Kallisto (43). Principal component and differential gene expression analyses were performed using DESeq2 (44). Change in gene expression between two conditions was defined as significant if absolute log2 fold change > 0.5 and FDR<5%. ComplexHeatmap package was used to generate heatmap (45). Enrichr (46, 47) was used for gene co-expression, GO molecular function 2018, KEGG 2019 Mouse and WikiPathways 2019 Mouse enrichment analyses. Significance of overlap between gene sets was tested using GeneOverlap package (http://shenlab-sinai.github.io/shenlab-sinai/).

Analysis of ATAC-seq datasets

ATAC-seq reads were mapped to the mm9 mouse genome using Bowtie2 (48). Paired reads with up to 2 kb separation were used (-X2000). Positions of Tn5 inserts were determined as a read start position offset by +4 bp for reads aligned to + strand and as a read start position offset by -5 bp for reads aligned to – strand (42). MACS2 (49) was used for peak calling with Tn5 inserts positions as input. The following parameters were

used --shift -75 --extsize 150 --nomodel -p 0.01. Peaks were merged across all conditions using bedtools (50). Principal component analysis and differential peak calling were performed using DESeq2 (44). Change in gene expression between two conditions was defined as significant if absolute log2 fold change > 0.5 and FDR<5%. Peaks were assigned to the genes with the nearest promoter. Genomic annotations were visualized using ChIPseeker package (51). Motif enrichment analysis was performed using findMotifsGenome.pl from HOMER suite (52) with default parameters.

Mouse mRNA primers

Gapdh FWD: CTGACGTGCCGCCTGGAGAAAC
Gapdh REV: CCCGGCATCGAAGGTGGAAGAGT
Baf53a/Actl6a FWD: GTGTACGGCGGAGATGAAGTT
Baf53a/Actl6a REV: GGGAAATCAACCTTAGGGCAGT
Baf53b/Actl6b FWD: GACGGAGCTGATGTTCGAGC
Baf53b/Actl6b REV: CTGTGGAGCGTCCATTTGC
Fos FWD: CGGGTTTCAACGCCGACTA
Fos REV: TTGGCACTAGAGACGGACAGA
Fosb FWD: TTTTCCCGGAGACTACGACTC
Fosb REV: GTGATTGCGGTGACCGTTG
Fosl2 FWD: CCAGCAGAAGTTCCGGGTAG
Fosl2 REV: GTAGGGATGTGAGCGTGGATA
Jun FWD: AGCCTACCAACGTGAGTGCT
Jun REV: AGAACGGTCCGTCACTTCAC
Junb FWD: TTTTGTCAAAGCCCTGGACG
Junb REV: GGGGAGTAACTGCTGAGGTT
Npas4 FWD: CAGATCAACGCCGAGATTCG
Npas4 REV: CACCCTTGCGAGTGTAGATGC
Nr4a1 FWD: GTTATCCGAAAGTGGGCAGA
Nr4a1 REV: AGTACCAGGCCTGAGCAGAA
Ier2 FWD: TGACTCTGTCGGTATGGAAGAT
Ier2 REV: ACCTTGGCTGAGAGGTAGACC
Egr1 FWD: TCGGCTCCTTTCCTCACTCA
Egr1 REV: CTCATAGGGTTGTTCGCTCGG
Egr3 FWD: CCGGTGACCATGAGCAGTTT
Egr3 REV: TAATGGGCTACCGAGTCGCT
Egr4 FWD: CGCGCAGTGACGAGAAGAA
Egr4 REV: GAGAGGCCCAGCGAGTAGA
Arc FWD: AAGTGCCGAGCTGAGATGC
Arc REV: CGACCTGTGCAACCCTTTC
Dusp5 FWD: AGCGTGGTCTCTCCCAACTT
Dusp5 REV: GGTACGGAATGTGCAGTAGGT
Dusp6 FWD: ATAGATACGCTCAGACCCGTG
Dusp6 REV: ATCAGCAGAAGCCGTTCGTT
Bdnf exon 4 FWD: CAGGAGTACATATCGGCCACCA
Bdnf exon 4 REV: GTAGGCCAAGTTGCCTTGTCCGT

Vgf FWD: AAGGATGACGGCGTACCAGA
Vgf REV: TGCCTGCAACAGTACCGAG
Nptx2 FWD: CTCAAGGACCGCTTGGAGAG
Nptx2 REV: GGTCTCATTATGAAGCAGGGAC
Txnip (transcript var2) FWD: TCTTTTGAGGTGGTCTTCAACG
Txnip (transcript var2) REV: GCTTTGACTCGGGTAACTTCACA
Major Satellite FWD: GACGACTTGAAAAATGACGAAATC
Major Satellite REV: CATATTCCAGGTCCTTCAGTGTGC
Minor Satellite FWD: CATGGAAAATGATAAAAACC
Minor Satellite REV: CATCTAATATGTTCTACAGTGTGG
LINE FWD: TTTGGGACACAATGAAAGCA
LINE REV: CTGCCGTCTACTCCTCTTGG
IAP FWD: TTGATAGTTGTGTTTTAAGTGGTAAATAAA
IAP REV: AAAACACCACAAACCAAAATCTTCTAC

Human mRNA primers
GAPDH FWD: ACCACAGTCCATGCCATCAC
GAPDH REV: TCCACCACCCTGTTGCTGTA
BAF53a/ACTL6A FWD: GGAGTCAGTCATGTTGTCAC
BAF53a/ACTL6A REV: CTCCGTTCCACTGTTGTATT
BAF53b/ACTL6B FWD: CCCTCAAGAATGGCATGAT
BAF53b/ACTL6B REV: ACAGCCGTCTTGCATAAG
FOS FWD: TCCAGTGCCAACTTCATTC
FOS REV: CCTGTCATGGTCTTCACAAC
FOSB FWD: GAGAAGGAACGTCTGGAGTTTG
FOSB REV: CTAAGGAAGATGGCTTCAGCTG
FOSL2 FWD: CGAACCTCGTCTTCACCTATC
FOSL2 REV: CATCAGACTCCTTGAACTCCC
JUN FWD: CCGAGAGCGGACCTTAT
JUN REV: CGTTGCTGGACTGGATTAT
VGF FWD: CTGAGCATAAAGAGCCGGTAG
VGF REV: AGGACGAGGGAGAGCTTT
DUSP5 FWD: CTGAGTGTTGCGTGGATGTA
DUSP5 REV: TAAATGTCAGCTACAGGCCAG

Statistics
For the behavioral experiments in this study, investigators were blinded to mouse genotype during data acquisition and analysis. No statistical method was used to predetermine sample size. One-way ANOVA with Tukey's *post hoc* correction was used to compare multiple groups for a single variable. To assess significant differences in the expression of mutant protein or mRNA relative to wild type, an ordinary one-way ANOVA with Dunnett's correction was employed. Where only two groups were compared, a two-tailed student's t-test was used. Whiskers for box and whisker plots represented the 10^{th} and 90^{th} percentiles. Error bars were plotted as standard error of the mean (s.e.m.) and differences were considered significant when $P < 0.05$. Unless

otherwise specified, *n* indicates biological replicates. For RNA- and ATAC-sequencing data, adjusted *P* values data were obtained using Bonferroni correction for multiple comparisons and significant differences were was defined as false discovery rate (FDR)<5% and with log2 fold changes>0.5. The significance of overlaps between datasets (gene set enrichment analysis) was performed using hypergeometric tests, where *P* indicates adjusted significance after Bonferroni correction for multiple comparisons. Statistical analyses were performed using Prism 6.0 (GraphPad Software), or using software described in "Analysis of RNA-seq Datasets**"**. All data were found to exhibit normality and equal variances.

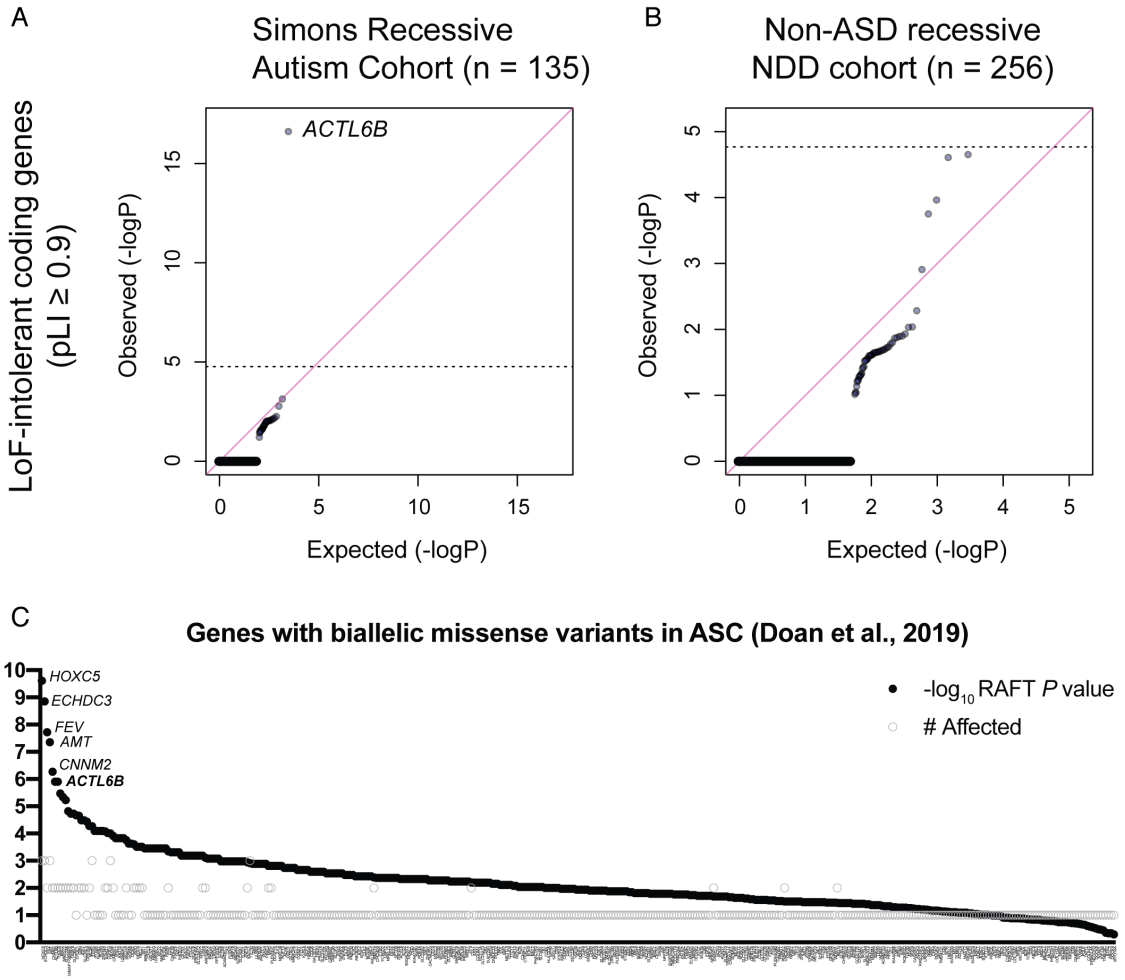

Fig. S1. *ACTL6B* is significantly mutated in two recessive autism cohorts.
(A) QQ plot showing the observed/expected # mutations in the recessive ASD cohort for genes that are do not tolerate mutation in the greater human population (indicated by pLI>0.9). *ACTL6B* stands out as the only significant gene in the cohort. *(B)* QQ plot showing the observed/expected # mutations in a non-ASD recessive brain disease cohort for genes that do not tolerate mutation in the greater human population (indicated by pLI>0.9). *ACTL6B* is not enriched, indicating a specific role in ASD. *(C)* Doan and colleagues identified 409 genes with recessive missense variants in the Autism Sequencing Consortium (ASC). These genes are shown rank-ordered by their RAFT P value, a measure of how significantly the gene was mutated. *ACTL6B* was the sixth most significantly mutated gene and was associated with missense variants in 2 affected individuals.

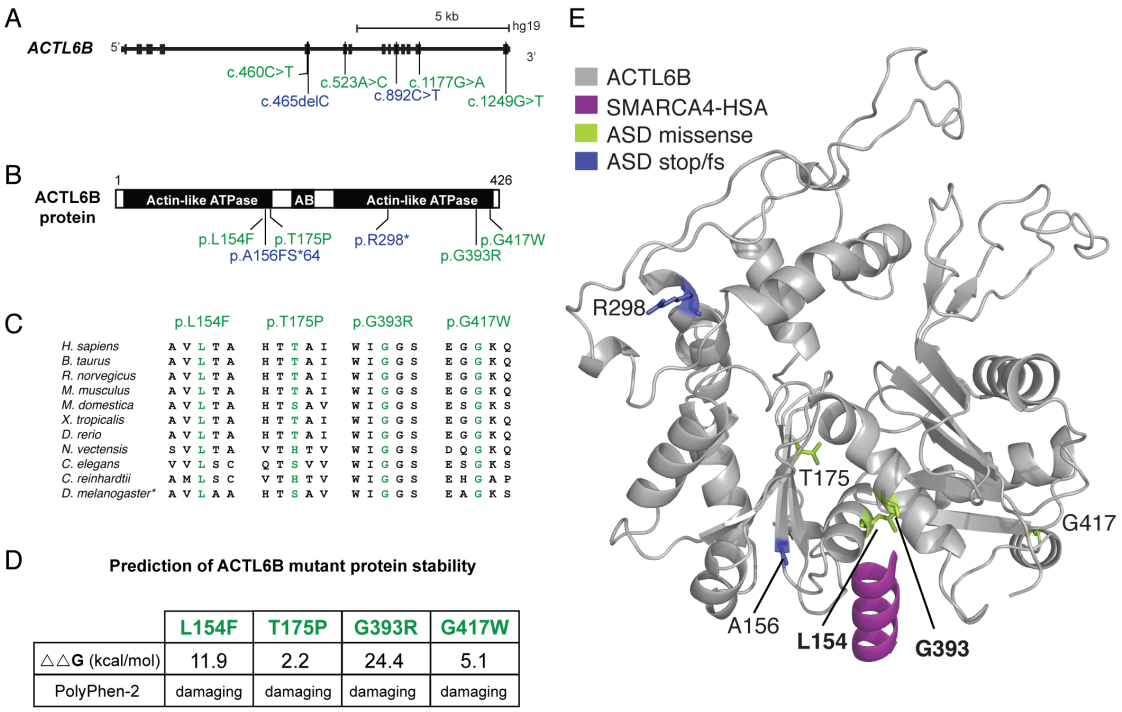

	L154F	T175P	G393R	G417W
△△G (kcal/mol)	11.9	2.2	24.4	5.1
PolyPhen-2	damaging	damaging	damaging	damaging

Fig. S2. Patient mutations are predicted to disrupt ACTL6B protein stability.
(A) Genomic and *(B)* protein domains with location of *ACTL6B* variants. *(C)* Sequence conservation across missense variants, altered charge inside of conserved motifs. *(D) In silico* prediction of ACTL6B missense mutant protein stability relative to wildtype. Calculated difference in Gibb's free energy of protein folding for missense mutant ACTL6B proteins relative to wild type indicates that more energy is required to fold missense mutant proteins. PolyPhen-2 protein stability prediction software predicts that missense mutations will be damaging. *(E)* Protein model of human ACTL6B (gray) bound to the SMARCA4 alpha-helical HSA domain (purple). Missense mutated residues L154 and G393 stabilize the barbed end structure that engages SMARCA4-HSA (bold).

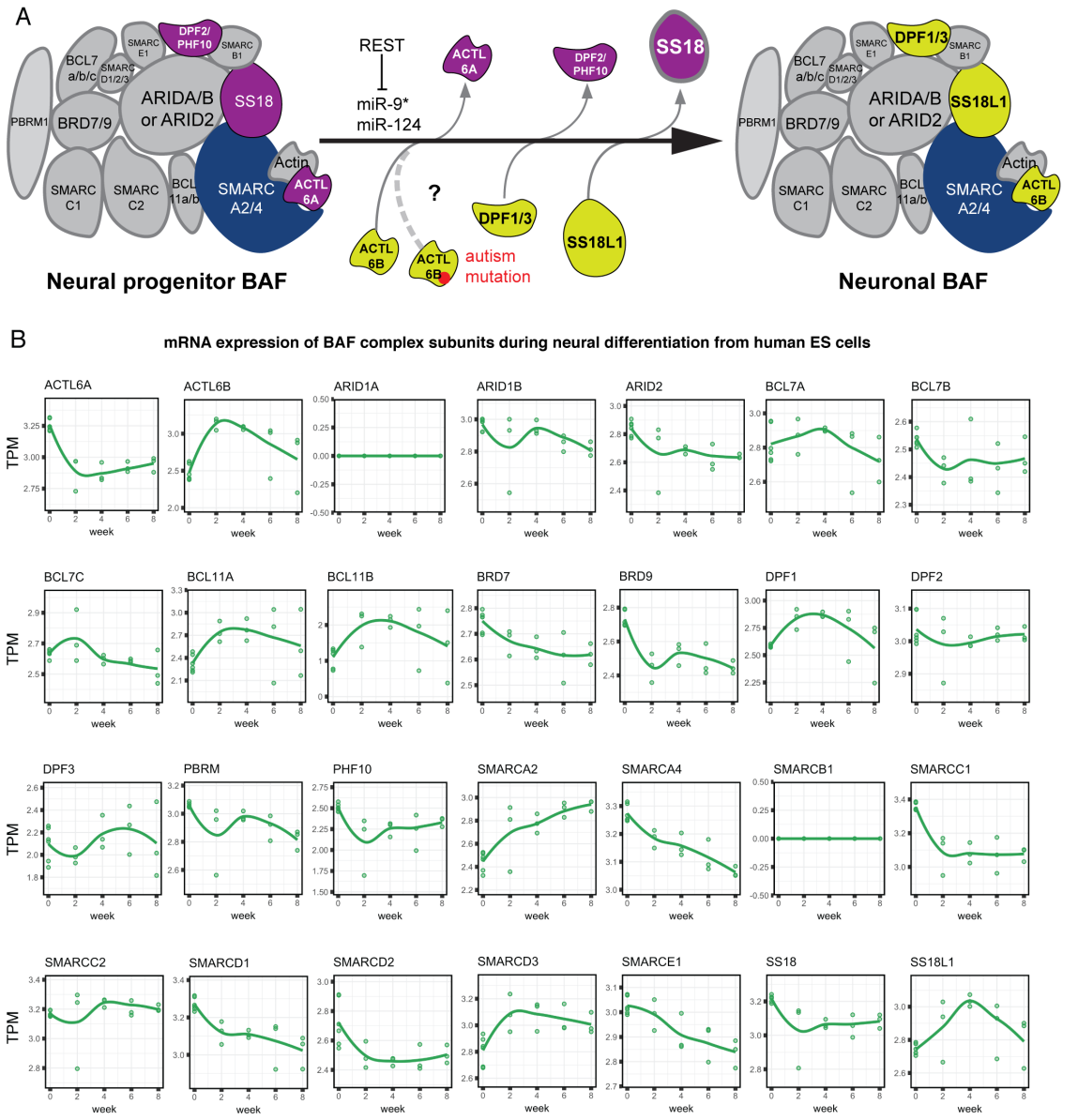

Fig. S3. BAF subunit exchange is conserved in human neural development.
(A) Model of subunit exchange in the BAF complex during neural differentiation transitioning from neural progenitor BAF to ACTL6B-containing neuronal BAF. *(B)* Comparison of TPM (Transcripts Per Million) from human neural precursor stage (week 0) to differentiated neuron stage (8 weeks) in vitro. Individual results from three or more replicates per condition. *ACTL6A* acutely decreased while *ACTL6B* increased during neural differentiation.

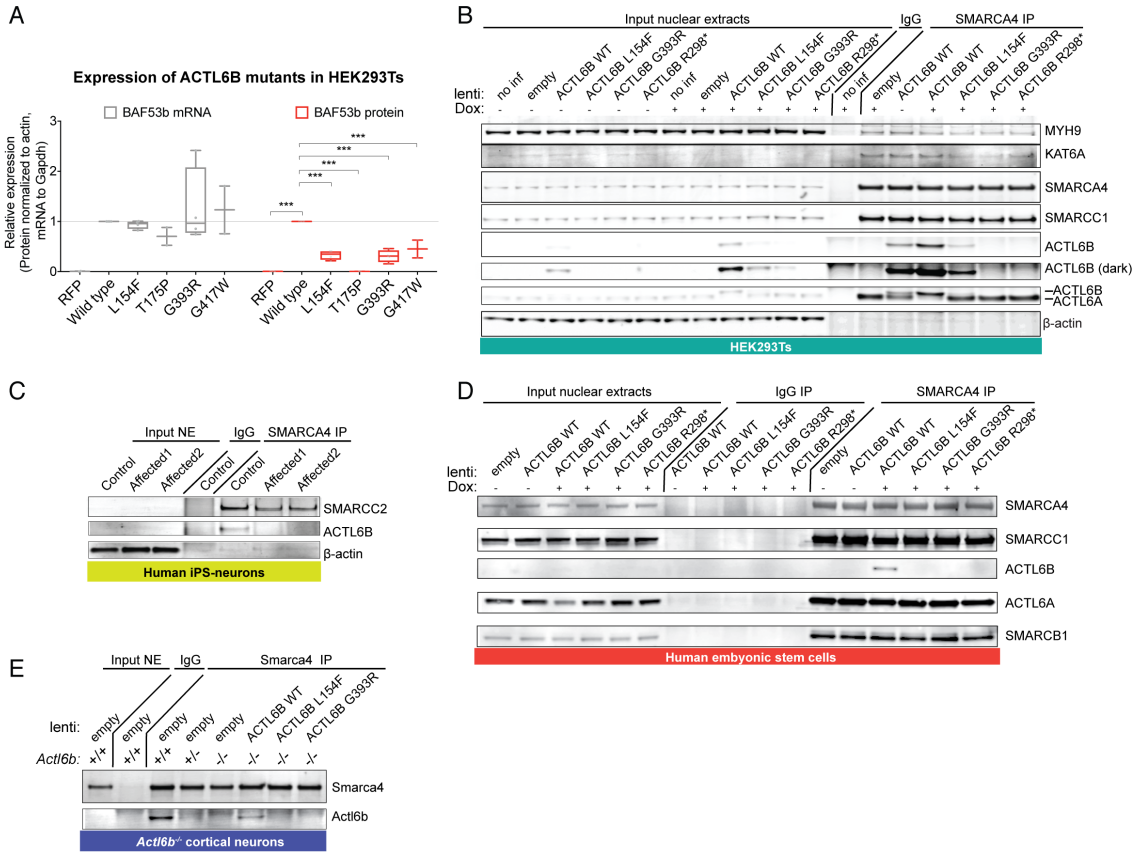

Fig. S4. Autism mutant ACTL6B proteins show reduced expression and representation in BAF complexes. *(A)* Mutant ACTL6B protein but not mRNA was significantly reduced relative to wildtype in transduced HEK293T cells, n=2 independent experiments for T175P and G417W, n=4 for wild type, L154F, G393R. Co-immunoprecipitation of human wildtype or mutant ACTL6B with BAF complexes from *(B)* transduced HEK293T cells, n=2; *(C)* wild type or affected (*ACTL6B*$^{L154F/L154F}$) induced pluripotent stem cell (iPS)-derived neurons, n=1; *(D)* transduced H9 human embryonic stem cells, n=1; *(E)* E18.5/DIV22 (transduced on DIV5) *Actl6b*$^{-/-}$ primary mouse embryonic cortical neurons, n=1. Note reduced or absent incorporation of patient mutant ACTL6B in all BAF complexes. Significance for (A) was calculated independently for mRNA or protein using an ordinary one-way ANOVA with Dunnett's correction for multiple comparisons. Whiskers indicate 10th and 90th percentiles. *P < 0.05; **P < 0.01, ***P < 0.001.

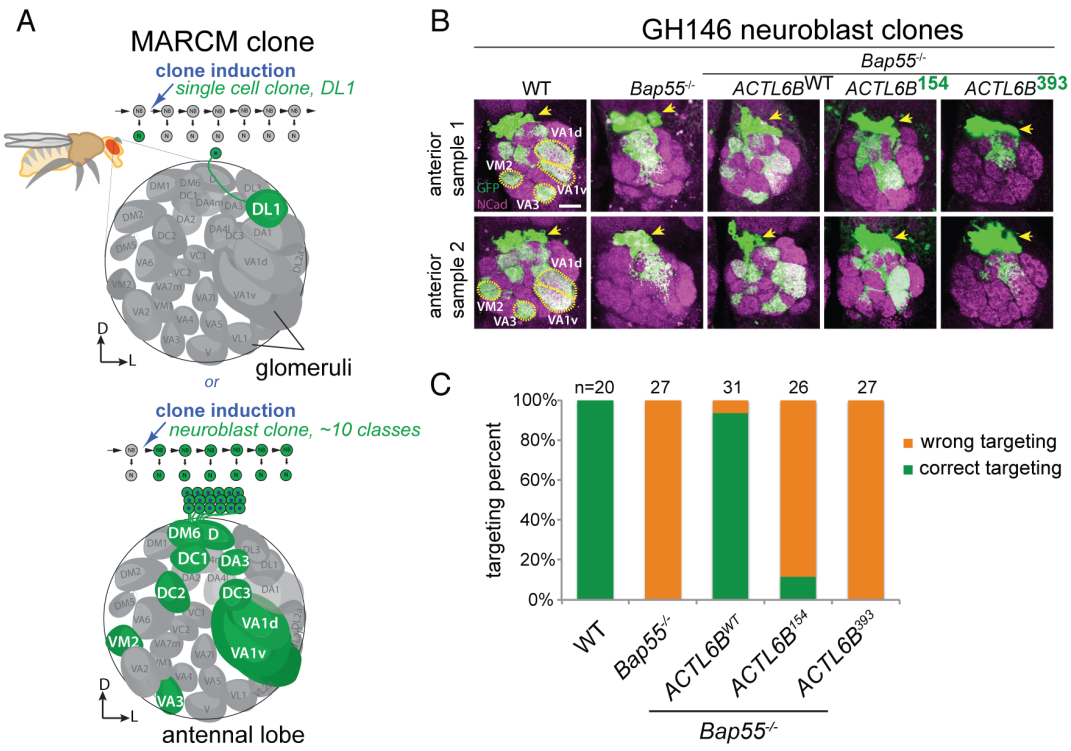

Fig. S5. Patient mutations cause a loss of function dendritic mistargeting phenotype in the fly olfactory system. *(A)* Diagram depicting method to assess *ACTL6B* mutant loss of function *in vivo* in fly olfactory system. MARCM: Mosaic Analysis with a Repressible Cell Marker was used to fluorescently label and replace fly *Bap55* with human *ACTL6B* alleles in olfactory projection neurons (PNs). PNs always project a dendrite to the dorsolateral glomerulus (DL1) in the posterior antennal lobe. Clones were induced in GH146-GAL4 flies at a time when DL1 PNs were born, so that two types of clones were generated: single cell clones targeting dendrites to DL1 glomerulus in the posterior antennal lobe and neuroblast clones consisting of ~10 classes of PNs targeting to different glomeruli. (*B)* Replacement of the fly orthologue *Bap55* with human wild type *ACTL6B* but not patient variants (L154F or G393R) rescued dendritic targeting of neuroblast clones. Arrows: cell bodies; Ncad: neuropil marker. Scale, 20 µm. (*C*) Quantification of (B) where correct targeting meant all 4 glomeruli were targeted as expected. n = animals per condition.

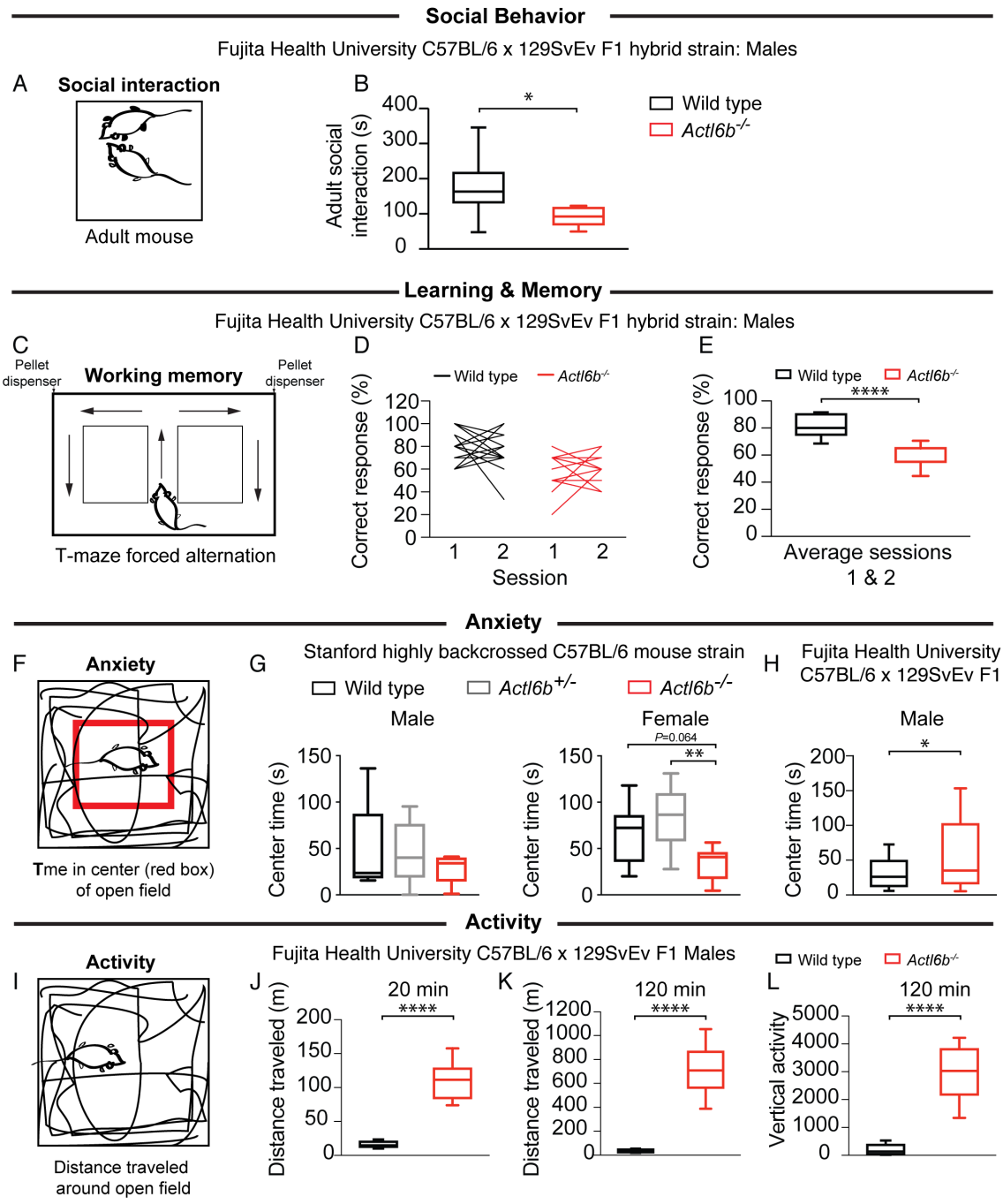

Fig. S6. *Actl6b*$^{-/-}$ mice exhibit social and memory deficits and hyperactivity.
(A) Diagram of social interaction test between male test mouse and stranger adult male of the same genotype. *(B) Actl6b*$^{-/-}$ mice show significantly reduced adult social interactions compared to wildtype mice. *(C)* Diagram depicting the T-maze forced alternation test for working memory. Correct response: choosing the arm opposite to the one where it received its previous food pellet. *(D)* Performance on the T-maze forced alternation test over two sessions. *(E)* Average performance of wild type vs *Actl6b*$^{-/-}$ mice on the T-maze forced alternation test indicates impaired working memory in the knockout mouse. *(F)* Diagram of open field test for anxiety: time spent in the 20 cm x 20 cm center (indicated

by red box) of a 40 cm x 40 cm open field over 20 minutes. *(G)* Pure C57BL/6 cohort: anxiety was significantly different between *Actl6b*$^{+/-}$ and *Actl6b*$^{-/-}$ females only. *(H)* 129S6/SvEV x C57BL/6 F1 cohort: knockout mice showed less anxiety relative to wildtype. *(I)* Diagram depicting the open field test. Total distance traveled in an open field over *(J)* 20 min or *(K)* 120 min indicates significant hyperactive phenotype in the knockout mouse. *(L)* *Actl6b*$^{-/-}$ mice showed more rearing behavior relative to wildtype. Male mice from the 129S6/SvEV x C57BL/6 F1 cohort in (B) were n=10 wildtype and n=10 *Actl6b*$^{-/-}$, and in (D, E, H-L) n=22 wildtype and n=21 *Actl6b*$^{-/-}$. Mice from the C57BL/6 cohort by genotype (+/+, +/-, -/-) shown in (G): n = 15, 18, 8 males, n = 11, 12, 9 females. Values were: $t_{18} = 2.53$ for (B), $F_{1,34} = 34.70$ for (D and E), F(2,38)=1.53 for males and F(2,29)=7.40 for females in (G), $t_{41}=2.27$ for (H), $t_{41}=13.50$ for (J), $t_{41}=13.01$ for (K), $t_{41}=8.88$ for (L). Significance for (G) was calculated using a one-way ANOVA with Tukey's multiple comparison post-hoc. Significance for all other tests was calculated with Student's t-test. Whiskers indicate 10th and 90th percentiles. **P* < 0.05; ***P* < 0.01, ****P* < 0.001, **** *P* < 0.0001.

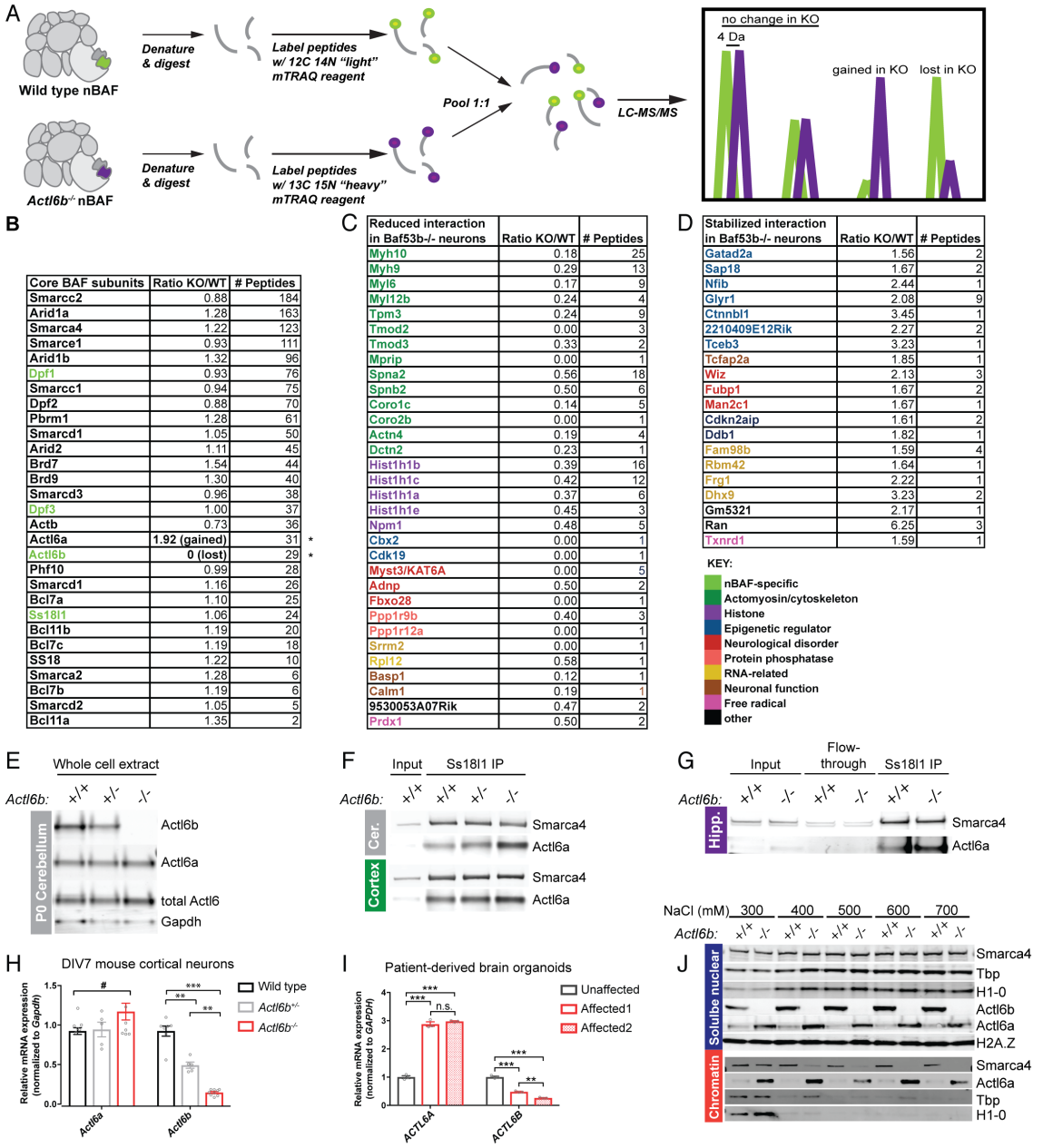

Core BAF subunits	Ratio KO/WT	# Peptides	
Smarcc2	0.88	184	
Arid1a	1.28	163	
Smarca4	1.22	123	
Smarce1	0.93	111	
Arid1b	1.32	96	
Dpf1	0.93	76	
Smarcc1	0.94	75	
Dpf2	0.88	70	
Pbrm1	1.28	61	
Smarcd1	1.05	50	
Arid2	1.11	45	
Brd7	1.54	44	
Brd9	1.30	40	
Smarcd3	0.96	38	
Dpf3	1.00	37	
Actb	0.73	36	
Actl6a	1.92 (gained)	31	*
Actl6b	0 (lost)	29	*
Phf10	0.99	28	
Smarcd1	1.16	26	
Bcl7a	1.10	25	
Ss18l1	1.06	24	
Bcl11b	1.19	20	
Bcl7c	1.19	18	
SS18	1.22	10	
Smarca2	1.28	6	
Bcl7b	1.19	6	
Smarcd2	1.05	5	
Bcl11a	1.35	2	

Reduced interaction in Baf53b-/- neurons	Ratio KO/WT	# Peptides
Myh10	0.18	25
Myh9	0.29	13
Myl6	0.17	9
Myl12b	0.24	4
Tpm3	0.24	9
Tmod2	0.00	3
Tmod3	0.33	2
Mprip	0.00	1
Spna2	0.56	18
Spnb2	0.50	6
Coro1c	0.14	5
Coro2b	0.00	1
Actn4	0.19	4
Dctn2	0.23	1
Hist1h1b	0.39	16
Hist1h1c	0.42	12
Hist1h1a	0.37	6
Hist1h1e	0.45	3
Npm1	0.48	5
Cbx2	0.00	1
Cdk19	0.00	1
Myst3/KAT6A	0.00	5
Adnp	0.50	2
Fbxo28	0.00	1
Ppp1r9b	0.40	3
Ppp1r12a	0.00	1
Srrm2	0.00	1
Rpl12	0.58	1
Basp1	0.12	1
Calm1	0.19	1
9530053A07Rik	0.47	2
Prdx1	0.50	2

Stabilized interaction in Baf53b-/- neurons	Ratio KO/WT	# Peptides
Gatad2a	1.56	2
Sap18	1.67	2
Nfib	2.44	1
Glyr1	2.08	9
Ctnnbl1	3.45	1
2210409E12Rik	2.27	2
Tceb3	3.23	1
Tcfap2a	1.85	1
Wiz	2.13	3
Fubp1	1.67	2
Man2c1	1.67	1
Cdkn2aip	1.61	2
Ddb1	1.82	1
Fam98b	1.59	4
Rbm42	1.64	1
Frg1	2.22	1
Dhx9	3.23	2
Gm5321	2.17	1
Ran	6.25	3
Txnrd1	1.59	1

Fig. S7. *Actl6b*$^{-/-}$ nBAF complexes contain non-neuronal variant Actl6a and have reduced affinity for chromatin. *(A)* Diagram depicting mTRAQ labeling method to measure nBAF proteins from wildtype (WT) vs. *Actl6b*$^{-/-}$ (KO) P0 neurons by mass spectrometry. Labeled peptides from wildtype or *Actl6b*$^{-/-}$ complexes were pooled at 1:1 ratio. *(B-D)* nBAF protein interactions with a Protein Prophet Probability cutoff>0.95. Single peptides were included as a resource but require further validation. Ratio: ASAP ratio scores for "heavy" ($^{13}C^{15}N$) labeled *Actl6b*$^{-/-}$ peptides or "light" ($^{12}C^{14}N$) labeled wildtype peptides. # Peptides: the total number of pooled peptides from wildtype and *Actl6b*$^{-/-}$ nBAF complexes. *(B)* BAF core subunits (neural-specific subunits in yellow green), indicate that nBAF is intact except for Actl6a replacement of Actl6b in mutant nBAF (*). *(C)* Destabilized interactions with *Actl6b*$^{-/-}$ nBAF. *(D)* Stabilized interactions with *Actl6b*$^{-/-}$ nBAF. *(E)* Actl6a/b protein expression analysis in P0 cerebellar tissues

from littermates showing increased Actl6a protein levels in the knockout, n=1 (see also nuclear extracts shown in G and J). *(F-G)* Immunoprecipitation of nBAF from nuclear extracts of wildtype, *Actl6b*$^{+/-}$ and *Actl6b*$^{-/-}$ littermates with anti-Ss18l1 antibody showing that Actl6a incorporation increased with decreasing Actl6b gene dosage in P0 cerebellar, cortical, or hippocampal tissues. *(H)* E16.5/DIV7 mouse cortical neurons show 1.2-fold higher mRNA expression of *Actl6a* in the absence of *Actl6b*. *(I)* 28 day old human brain organoids from 2 affected siblings show 3-fold higher mRNA expression of *ACTL6A* relative to an unaffected family member, n=3 brain organoids per individual. The affected genotype was *ACTL6B*$^{L154F/L154F}$ and unaffected genotype was *ACTL6B*$^{L154F/+}$. ***j.*** nBAF complexes isolated from E18.5/DIV7 *Actl6b*$^{-/-}$ cortical neurons bound chromatin less tightly than wild type complexes in the presence of increasing salt (NaCl); n=2. Note diminished Smarca4 binding in the *Actl6b*$^{-/-}$ chromatin fraction in the presence of 400 mM NaCl. Mice shown in (H) (+/+, +/-, -/-): 6, 5, 9. Values were F (2, 17) = 2.303 for (H) and F (2, 6) = 399.7 for (I). Statistical significance for (H) and (I) was assessed by one-way ANOVA with Tukey's correction for multiple comparisons. Error bars indicate standard error of the mean (s.e.m.). *$P < 0.05$; **$P < 0.01$, ***$P < 0.001$. # indicates $P<0.05$ using the Student's t-test.

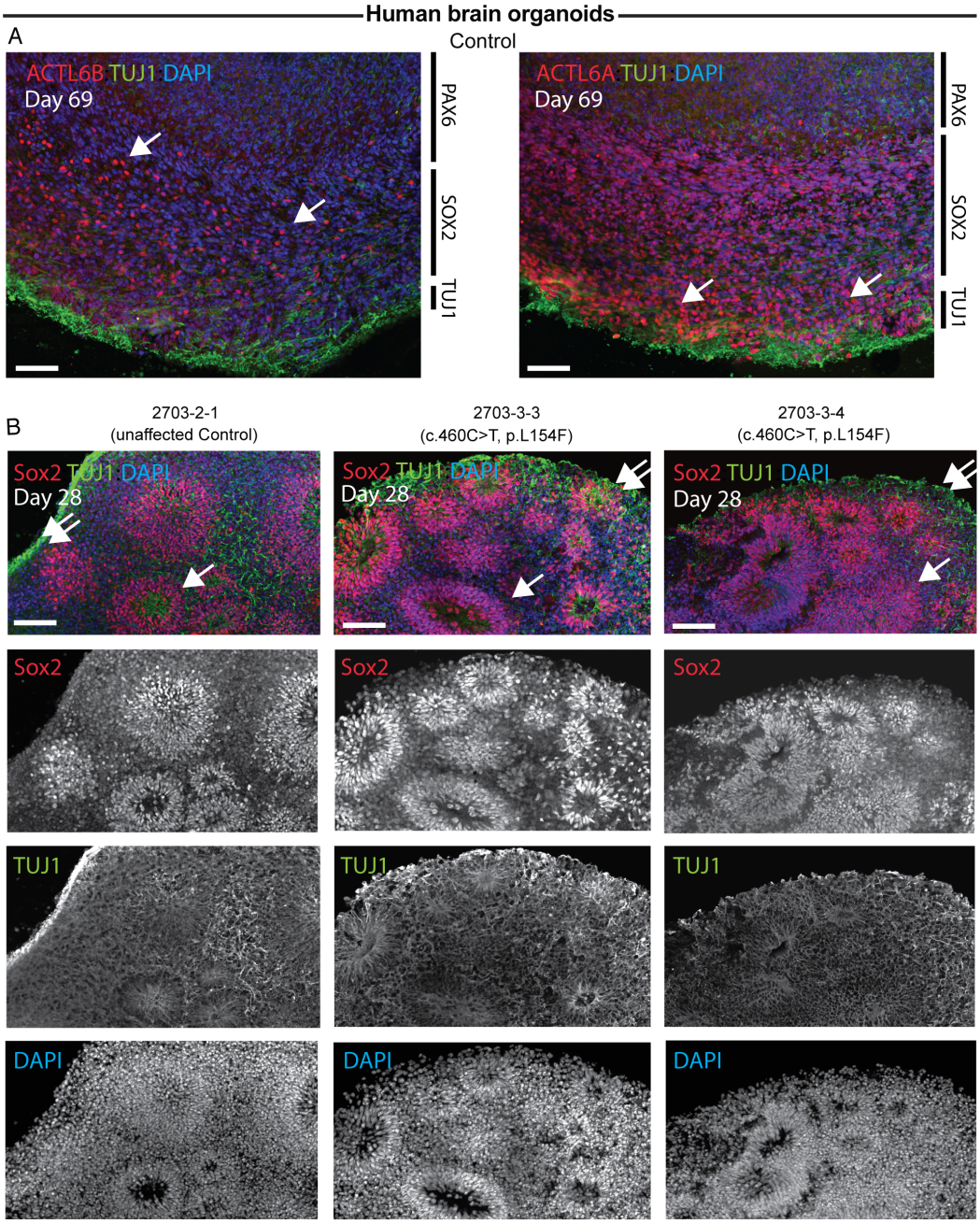

Fig. S8. Brain organoids from affected humans show similar expression of progenitor and immature neuronal markers to unaffected parent.
(A) Immunostaining of endogenous human ACTL6A and ACTL6B protein in day 69 wildtype brain organoids confirming expression in organoids. White arrows indicate specific ACTL6B or ACTL6A expression. Scale bar 50 uM. *(B)* Immunostaining for neural progenitor marker Sox2 and immature neuronal marker TUJ1 in brain organoids derived from 2 affected individuals of family 2703 with genotype ACTL6B$^{L154F/L154F}$ compared to organoid from unaffected parent (ACTL6B$^{L154F/+}$). Single arrows show Sox2+ rosettes, double arrows show TUJ1+ neural cells. Similar expression patterns and morphologies were seen, indicating that the organoids develop similarly by day 28.

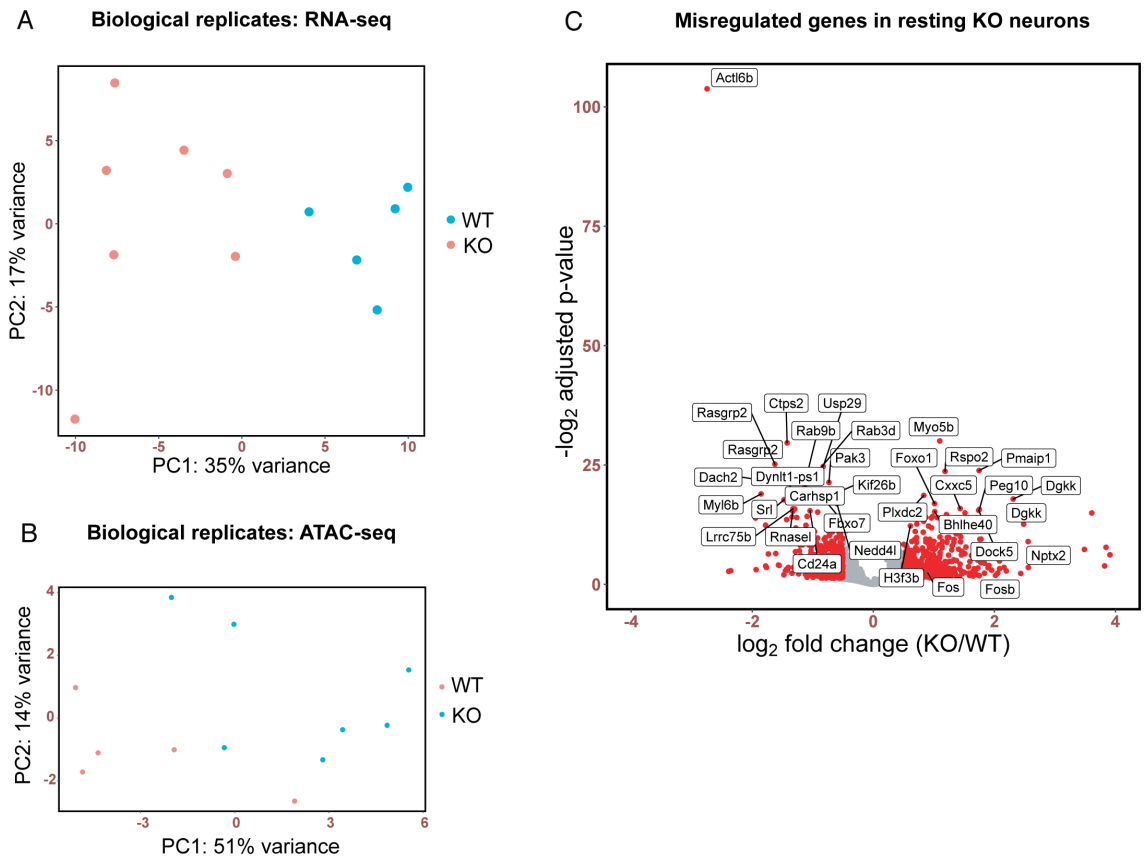

Fig. S9. Gene expression and chromatin accessibility in cortical cultures cluster by genotype. E16.5/DIV7 cortical cultures from n=5 wildtype or n=7 *Actl6b*$^{-/-}$ (KO) littermates were electrically silenced for 2 h with TTX/APV and collected for RNA- and ATAC-sequencing to measure basal transcription and chromatin accessibility, respectively. Principal component analysis was conducted on biological replicates examined by *(A)* RNA-sequencing or *(B)* ATAC-sequencing. *(C)* Volcano plot of gene expression changes in KO neurons relative to wildtype, where red dots indicate genes with FDR<5% and log2 fold change>0.5. The top 30 most significantly altered genes are labeled. *Actl6b* mRNA expression was significantly reduced in KO as expected.

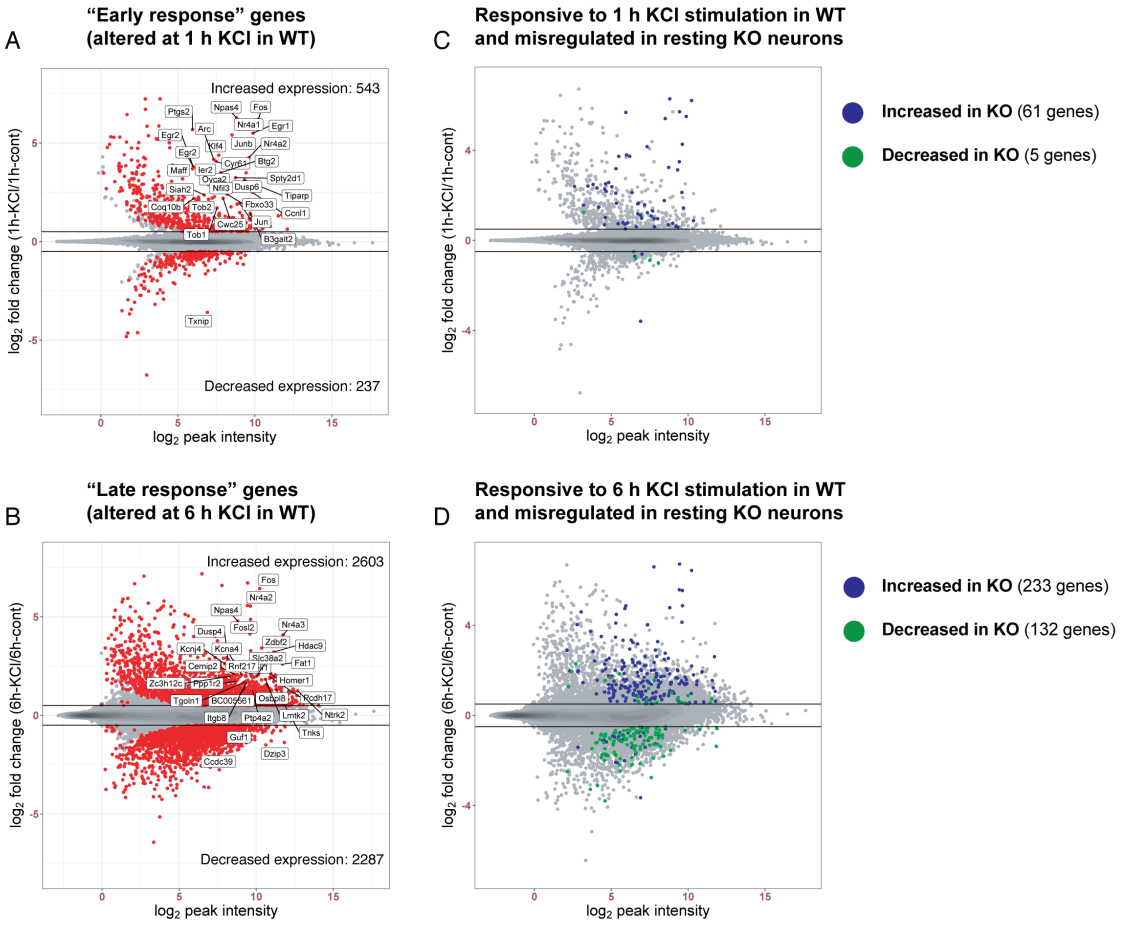

Fig. S10. Misregulated genes in resting *Actl6b*$^{-/-}$ neurons follow an activity-responsive expression pattern. Network activity in wildtype E16.5/DIV7 cortical cultures was silenced for 1 h with TTX/APV and then neurons were treated -/+55 mM KCl to depolarize neuronal membranes for 1 or 6 h. mRNA was examined by RNA-sequencing, n=5 biological replicates each for 1 h KCl and 1 h control, n=3 biological replicates for 6 h KCl and n=4 for 6 h control. *(A* and *B)* MA plots showing gene expression changes induced by 1 h or 6 h KCl stimulation in wildtype neurons. Red dots indicate genes whose expression was significantly altered by activity (FDR<5%, log2 fold change >0.5). The top 30 most significant gene names are labeled. *(C* and *D)* MA plots of 1 h or 6 h KCl-induced expression changes in wildtype, labeled with genes that were significantly increased (blue) or decreased (green) in resting *Actl6b*$^{-/-}$ (KO) neurons. Most genes that were significantly increased and decreased in resting KO neurons were likewise increased or decreased by KCl stimulation in wildtype.

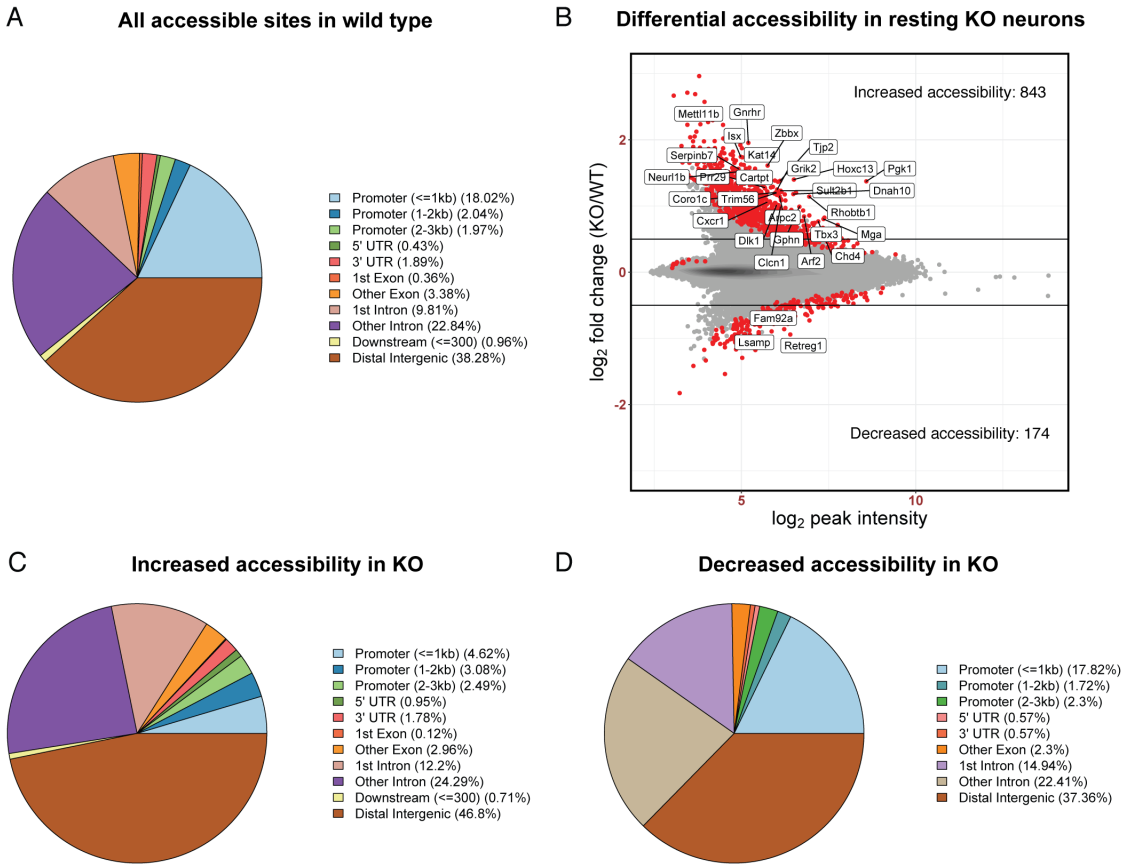

Fig. S11. Chromatin accessibility increased at distal intergenic regions in *Actl6b*$^{-/-}$ neurons. E16.5/DIV7 cortical cultures from n=5 wildtype or n=7 *Actl6b*$^{-/-}$ (KO) littermates were electrically silenced for 2 h with TTX/APV and transposed with Tn5 to measure chromatin accessibility by ATAC-sequencing. *(A)* Pie chart showing the distribution of accessible sites in wildtype neurons across the genome. Accessible sites in neurons are found predominantly in intergenic and intronic regions, with about 20% in promoters. *(B)* MA plot showing differential chromatin accessibility in KO neurons relative to wildtype. Significantly altered sites (FDR<5%, log2 fold change >0.5) are labeled in red. The top 30 most significantly altered sites in KO are labeled with the name of the nearest gene. Accessibility was predominantly increased in KO. *(C* and *D)* Pie charts showing the genomic distribution of accessibile sites that showed increased or decreased accessibility in KO. Sites that gained accessibility showed special enrichment at distal intergenic regions while those that lost accessibility showed special enrichment in introns.

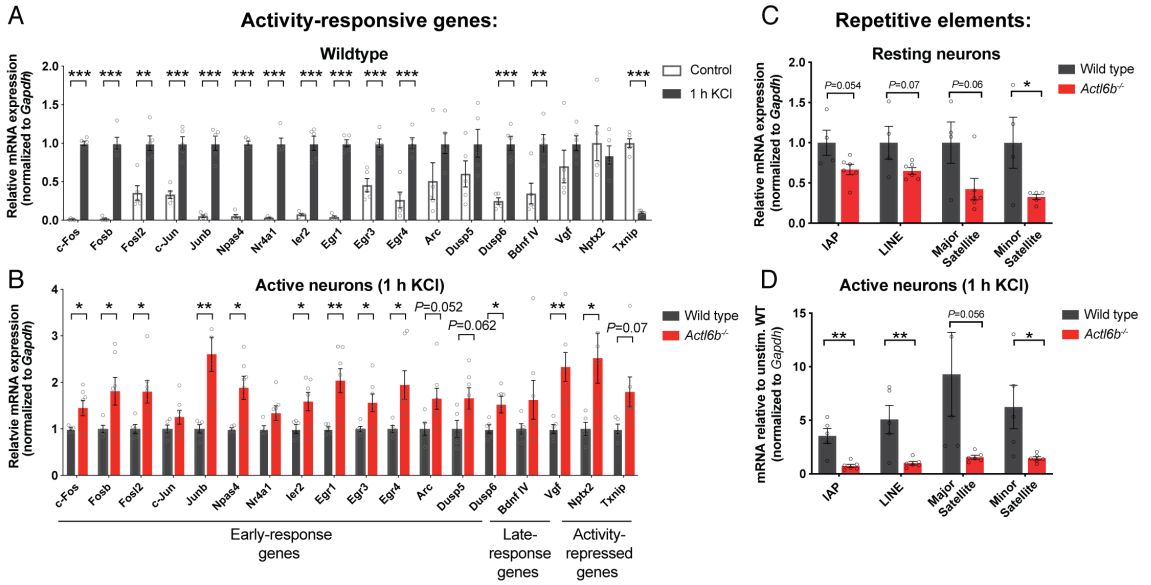

Fig. S12. The loss of Actl6b relieves repression on activity responsive genes but increases repression on repetitive elements. E16.5/DIV7 cortical cultures from wildtype or *Actl6b*$^{-/-}$ littermates were electrically silenced for 1 h with TTX/APV and then treated -/+55 mM KCl for 1 h to depolarize neuronal membranes. RNA was collected, DNAse-treated, reverse-transcribed into cDNA and quantified by quantitative PCR *(A)* Classical activity-responsive genes show expected transcriptional responses to neural activity in wildtype neurons, n=5 biological replicates. *(B)* Classical activity-responsive genes show significantly elevated expression in *Actl6b*$^{-/-}$ relative to wildtype following 1 h KCl stimulation, n=5 wildtype, n=7 *Actl6b*$^{-/-}$ biological replicates. *(C)* Repetitive element mRNA expression in the absence of neural activity, n=4 wildtype and n=5 *Actl6b*$^{-/-}$ biological replicates. *(D)* Repetitive element mRNA expression following 1 h KCl stimulation indicates robust expression in wildtype but not in *Actl6b*$^{-/-}$, n=5 wildtype and n=6 *Actl6b*$^{-/-}$ biological replicates. Statistical significance was calculated independently for each gene using a Student's t-test. Error bars indicate s.e.m. *$P < 0.05$; **$P < 0.01$, ***$P < 0.001$.

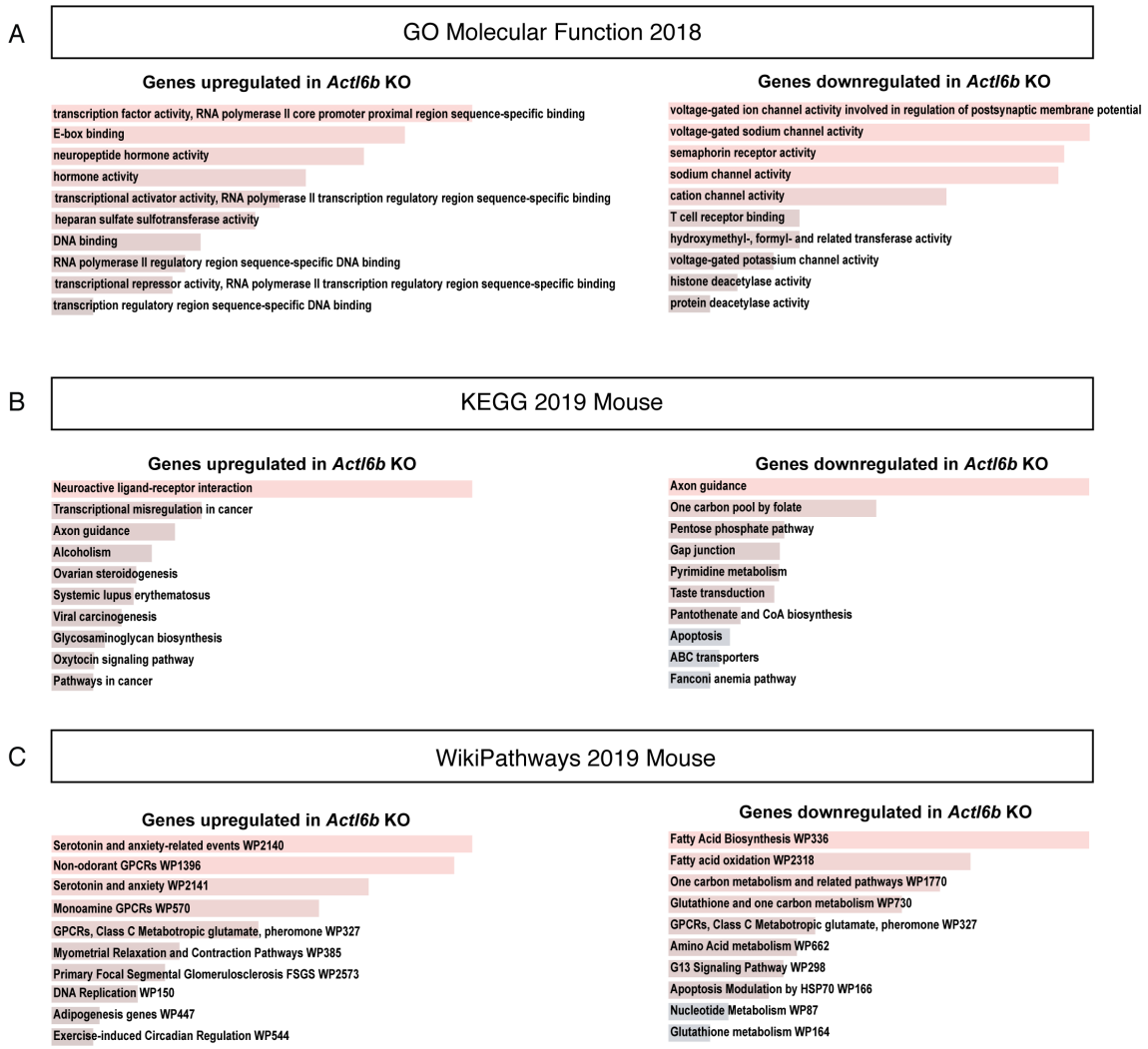

Fig. S13. Actl6b regulates the expression of genes related to the behavior, seizure, corpus callosum, and white matter phenotypes of affected humans. EnrichR analysis was conducted on *Actl6b*-regulated genes identified in our RNA-sequencing study of activity-silenced E16.5/DIV7 cultured cortical neurons from wildtype or *Actl6b*$^{-/-}$ littermates. *(A)* Gene ontology (GO) analysis of molecular functions of misregulated genes in *Actl6b*$^{-/-}$ neurons. Upregulated genes are associated with transcription and downregulated genes are enriched for genes that control ion balance and maintain membrane polarity. *(B)* KEGG functional analysis of misregulated genes in *Actl6b*$^{-/-}$. Upregulated genes are enriched for genes involved in synaptic transmission and downregulated genes are enriched for genes involved in axon guidance. *(C)* WikiPathways analysis indicates that genes in the serotonin pathway that regulate behavior are upregulated in *Actl6b*$^{-/-}$ neurons. Downregulated genes in *Actl6b*$^{-/-}$ neurons were involved in fatty acid biosynthesis, a process necessary for building lipid membranes.

Chr	Pos	Ref	Alt	Gene	cDNA	AAChange	GT Index	OMIM	AltAF Index	Reads Index	Qual Index	Func	Impact	Transcript	Segregate	Local Found	Sift Rank	Mut Taster Rank	Fathmm Rank
Family 2655 Sequenced father, mother and affected child																			
4	5448499	G	A	STK32B	c.662G>A	p.(Gly221Asp)	1/1		1	29	1494	missense	MOD	NM_018401.1	Y	3	0.65363	0.81033	0.39781
7	100243895	C	T	ACTL6B	c.1177G>A	p.(Gly393Arg)	1/1	612458	1	15	791	missense	MOD	NM_016188.4	Y	3	0.78421	0.81033	0.99905
9	32633273	C	A	TAF1L	c.2305G>T	p.(Ala769Ser)	1/1	607798	1	143	8961	missense	MOD	NM_153809.2	N	3	0.63171	0.50429	0.21285
9	77257692	A	G	RORB	c.598A>G	p.(Asn200Asp)	1/1	601972	1	39	2113	missense	MOD	NM_006914.3	N	3	0.21113	0.44871	0.9348
Family 2703 Sequenced two affected children																			
7	100247668	G	A	ACTL6B	c.460C>T	p.(Leu154Phe)	1/1	612458	1	23	1556	missense	MOD	NM_016188.4	Y	2	0.72092	0.81033	0.96374
Family 2727 Sequenced father, mother and affected child																			
1	11897497	C	G	CLCN6	c.2170C>G	p.(Leu724Val)	1/1	602726	1	62	3928	missense	MOD	NM_001256959.1	N	3	0.31046	0.81033	0.88158
7	100244638	G	A	ACTL6B	c.892C>T	p.(Arg298*)	1/1	612458	1	37	2326	stop_gained	HIGH	NM_016188.4	Y	3		0.81033	
Family 3816 Sequenced two affected children																			
7	100246391	T	G	ACTL6B	c.523A>C	p.(Thr175Pro)	1/1	612458	1	41	2207	missense	MOD	NM_016188.4	Y	2	0.63	0.59	0.98
16	4015881	T	A	ADCY9	c.3957A>T	p.(Glu1319Asp)	1/1	603302	1	180	10750	missense	MOD	NM_001116.3	N	2	0.91	0.38	0.84
17	73498246	G	C	CASKIN2	c.2663C>G	p.(Pro888Arg)	1/1	612185	1	102	5504	missense	MOD	NM_001142643.2	N	2	0.39	0.09	0.69
Family 4504 Sequenced one affected child																			
2	1914046	A	G	MYT1L	c.1777T>C	p.(Ser593Pro)	1/1	613084	1	40	1405	missense	MOD	NM_015025.2	Y	1	0.15588	0.42538	0.49364
2	182981991	C	T	PPP1R1C	c.299C>T	p.(Thr100Ile)	1/1	613240	1	42	1319	missense	MOD	NM_001080545.2	Y	1	0.22366	0.08979	0.28187
7	100247662-1	CG	C	ACTL6B	c.465del	p.(Thr155Thrfs*1	1/1	612458	1	30	1020	frameshift	HIGH	NM_016188.4	Y	1			
7	100486880	G	C	UFSP1	c.13C>G	p.(Pro5Ala)	1/1	611481	1	74	2549	missense	MOD	NM_001015072.3	N	2	0.36066	0.45633	0.47134
8	109797210	G	A	TMEM74	c.118C>T	p.(Leu40Phe)	1/1	613935	1	98	3349	missense	MOD	NM_153015.1	N	3	0.18794	0.24449	
8	125989175	G	C	ZNF572	c.665G>C	p.(Gly222Ala)	1/1		1	93	2983	missense	MOD	NM_152412.2	N	1	0.39526	0.35305	0.015
Family 5309 Sequenced one affected child																			
7	100240901	C	A	ACTL6B	c.1249G>T	p.(Gly417Trp)	1/1	612458	1	21	663	missense	MOD	NM_016188.4	Y	1	0.8689	0.09389	0.8342
19	50265383	T	A	TSKS	c.277A>T	p.(Thr93Ser)	1/1	608253	1	38	1807	missense	MOD	NM_021733.1	Y	3	0.232	0.24578	0.2745
X	9714171	C	T	GPR143	c.571G>A	p.(Ala191Thr)	1/1	300808	1	9	251	missense	MOD	NM_000273.2	N	1	0.1387	0.13875	0.13567
X	49067549	T	C	CACNA1F	c.4264A>G	p.(Ile1422Val)	1/1	300110	1	14	428	missense	MOD	NM_001256789.1	Y	1	0.34578	0.03967	0.2358

Table S1. Variant table from whole exome/genome sequencing

Variant tables resulting from whole exome/genome sequencing in each of the 6 families analyzed as part of this study. Family number and the individuals that underwent sequencing are listed at top. Each variant passing standard clinical filters (see Methods) is shown. Positions referenced to hg19. GT: genotype of the index. OMIM# is listed if assigned. AltAF: alternative allelic fraction. Reads Index: Read# from index subject. Func: predicted effect of variant on protein. Impact: Mod=moderate, Severe=severe. Transcript ID provided. Segregate: variant segregated according to a strict recessive mode of inheritance in the entire family. Y:yes; N: no. Local found: Instances of the allele among the internal database of 6000 exomes. Sift Rank, Mut Taster and Fathom Rank: damage predication score rankings. In each family, high-impact variants were prioritized. Genes with assigned non-nervous system function, expression, or without clinical overlap with these patients were deprioritized. In each family, *ACTL6B* was the only variant that segregated and remained after standard clinical variant prioritization.

Clinical Features of Individuals with Mutations in *BAF53b/ACTL6B*									
Patient	**2655 III:3**	**2703 III:3**	**2703 III:4**	**2703 III:5**	**2727 III:6**	**3816 III:3**	**3816 III:4**	**4504 III:2**	**5039 III:1**
Gender	female	male	male	female	male	female	male	male	male
Age at presentation	6 mos	18 mos	12 mos	3 mos	7 mos	3 y	1y	4 mos	3 mos
Country of origin	Pakistan	Pakistan	Pakistan	Pakistan	Egypt	Egypt	Egypt	Egypt	Egypt
Consanguinity	+	+	+	+	+	+	+	+	+
Mutation type	missense	missense	missense	missense	nonsense	missense	missense	frameshift	missense
Zygosity	homozygous	homozygous	homozygous	homozygous	homozygous	homozygous	homozygous	homozygous	homozygous
cDNA mutation	c.1177G>A	c.460C>T	c.460C>T	c.460C>T	c.892C>T	c.523A>C	c.523A>C	c.465delC	c.1249G>T
Protein alteration	p.Gly393Arg	p.Leu154Phe	p.Leu154Phe	p.Leu154Phe	p.Arg298*	p.Thr175Pro	p.Thr175Pro	p.Ala156fs*64	p.Gly417Trp
Neurological Findings									
Intellectual disability	+	+	+	+	+	+	+	+	+
Speech delay	No speech	No speech	No speech	No speech	No speech	No speech	No speech	No speech	No speech
Autistic features	+	+	+	+	+	+	+	+	+
Hyperactivity	+	+	+	+	+	+	+	+	+
Hypertonia	+	+	+	+	+	+	+	+	-
Epilepsy	Multifocal epilepsy at 1y	Myoclonic and focal seizures at 2m	Myoclonic and focal seizures at 3m	Myoclonic and focal seizures at 3w	Myoclonic and focal seizures at 1w	Myoclonic, tonic and focal at 2m controlled on valproate and vigabatrin	Myoclonic and focal at 2m, not controlled	Myoclonic at 1m Tonic seizures at 2.5m	GTC at 5y then atonic seizures at 6y, controlled on Valproate.
EEG	Diffuse epileptiform activity	NA	Diffuse epileptiform activity	NA	Burst suppression	Sucortical discharges	Subcortical discharge	Bilateral temporal focus	Diffuse epileptiform activity
Microcephaly	42.5cm (-3SD)	44.5cm (-2SD)	44cm (-2SD)	42cm (-3SD)	41 cm -3.8SD	42cm (-4SD)	41.5cm (-3.1SD)	38 cm (-2SD)	49.7cm (-1.7SD)
Developmental delay	+	+	+	+	+	+	+	+	+
Failure to thrive	+	+	+	+	+	+	+	+	+
Spasticity (mild)	+	+	+	+	+	+	+	+	-
Joint laxity	-	-	-	-	-	-	-	-	-
Other	Brisk reflexes	Spasticity and dystonia	Spasticity and dystonia	Spasticity and dystonia	Spastic, brisk reflexes, dystonia, nystagmus	Spastic, brisk reflexes, dystonia, poor vision, nystagmus, recurrent chest infection	Spastic, brisk reflexes, dystonia, poor vision, nystagmus, recurrent chest infection	Spastic, brisk reflexes, dystonia, poor vision, nystagmus, recurrent chest infection	Spasticity and dystonia
Cranial MRI Findings									
MRI	Cortical and cental atrophy. Hypogenesis of corpus callosum	Cortical and cental atrophy. Hypogenesis of corpus callosum	NA	NA	Cortical and cental atrophy. Hypogenesis of corpus callosum	Cortical and cental atroph Hypogenesis of corpus callosum	Cortical and cental atroph Hypogenesis of corpus callosum	Cortical and cental atrophy. Hypogenesis of corpus callosum	Cortical and cental atroph Hypogenesis of corpus callosum

Table S2. Clinical features of affected individuals with *ACTL6B* mutations MRI= magnetic resonance imaging; EEG= electroencephalography

Movie S1 (separate file, 2727.mp4). Behaviors of an affected child harboring homozygous loss of function variant in *ACTL6B*.
Movie clip of affected individual from family 2727 showing features consistent with autism, including absent language, motor automatisms, and posturing of upper extremities.

Movie S2 and S3 (separate files, MUTANT.mp4 and WILDTYPE.mp4). Behaviors of *Actl6b*$^{-/-}$ and *Actl6b*$^{+/+}$ littermates.
Representative home-cage movie clip demonstrating degree of hyperactivity in *Actl6b*$^{-/-}$ mutants.

Dataset S1. Transcriptional changes in wildtype and *Actl6b*$^{-/-}$ neurons.
Processed RNA-sequencing datasets from wildtype or *Actl6b*$^{-/-}$ cultured primary E16.5/DIV7 mouse cortical neurons.

Dataset S2. Chromatin accessibility changes in *Actl6b*$^{-/-}$ neurons.
Processed RNA-sequencing datasets from wildtype or *Actl6b*$^{-/-}$ cultured primary E16.5/DIV7 mouse cortical neurons.

Dataset S3. Original western blots and replicate experiments.
This file contains raw western blot scans and experimental replicates.

References

1. Novarino G*, et al.* (2014) Exome sequencing links corticospinal motor neuron disease to common neurodegenerative disorders. *Science* 343(6170):506-511.
2. Chambers SM*, et al.* (2009) Highly efficient neural conversion of human ES and iPS cells by dual inhibition of SMAD signaling. *Nature biotechnology* 27(3):275-280.
3. Schaffer AE*, et al.* (2018) Biallelic loss of human CTNNA2, encoding alphaN-catenin, leads to ARP2/3 complex overactivity and disordered cortical neuronal migration. *Nature genetics*.
4. Bardy C*, et al.* (2015) Neuronal medium that supports basic synaptic functions and activity of human neurons in vitro. *Proceedings of the National Academy of Sciences of the United States of America* 112(20):E2725-2734.
5. Kadoshima T*, et al.* (2013) Self-organization of axial polarity, inside-out layer pattern, and species-specific progenitor dynamics in human ES cell-derived neocortex. *Proceedings of the National Academy of Sciences of the United States of America* 110(50):20284-20289.
6. Wu JI*, et al.* (2007) Regulation of dendritic development by neuron-specific chromatin remodeling complexes. *Neuron* 56(1):94-108.
7. Gunaydin LA*, et al.* (2014) Natural neural projection dynamics underlying social behavior. *Cell* 157(7):1535-1551.

8. Katayama Y*, et al.* (2016) CHD8 haploinsufficiency results in autistic-like phenotypes in mice. *Nature* 537(7622):675-679.
9. Kaidanovich-Beilin O, Lipina T, Vukobradovic I, Roder J, & Woodgett JR (2011) Assessment of social interaction behaviors. *Journal of visualized experiments : JoVE* (48).
10. Miyakawa T*, et al.* (2001) Neurogranin null mutant mice display performance deficits on spatial learning tasks with anxiety related components. *Hippocampus* 11(6):763-775.
11. Seibenhener ML & Wooten MC (2015) Use of the Open Field Maze to measure locomotor and anxiety-like behavior in mice. *Journal of visualized experiments : JoVE* (96):e52434.
12. Maze I*, et al.* (2015) Critical Role of Histone Turnover in Neuronal Transcription and Plasticity. *Neuron* 87(1):77-94.
13. Ataman B*, et al.* (2016) Evolution of Osteocrin as an activity-regulated factor in the primate brain. *Nature* 539(7628):242-247.
14. Bartel DP, Sheng M, Lau LF, & Greenberg ME (1989) Growth factors and membrane depolarization activate distinct programs of early response gene expression: dissociation of fos and jun induction. *Genes & development* 3(3):304-313.
15. Meerbrey KL*, et al.* (2011) The pINDUCER lentiviral toolkit for inducible RNA interference in vitro and in vivo. *Proceedings of the National Academy of Sciences of the United States of America* 108(9):3665-3670.
16. Lessard J*, et al.* (2007) An essential switch in subunit composition of a chromatin remodeling complex during neural development. *Neuron* 55(2):201-215.
17. Stanton BZ*, et al.* (2017) Smarca4 ATPase mutations disrupt direct eviction of PRC1 from chromatin. *Nature genetics* 49(2):282-288.
18. Olave I, Wang W, Xue Y, Kuo A, & Crabtree GR (2002) Identification of a polymorphic, neuron-specific chromatin remodeling complex. *Genes & development* 16(19):2509-2517.
19. Gillespie MA*, et al.* (2015) An LXR-NCOA5 gene regulatory complex directs inflammatory crosstalk-dependent repression of macrophage cholesterol efflux. *The EMBO journal* 34(9):1244-1258.
20. Keller A, Nesvizhskii AI, Kolker E, & Aebersold R (2002) Empirical statistical model to estimate the accuracy of peptide identifications made by MS/MS and database search. *Anal Chem* 74(20):5383-5392.
21. Nesvizhskii AI, Keller A, Kolker E, & Aebersold R (2003) A statistical model for identifying proteins by tandem mass spectrometry. *Anal Chem* 75(17):4646-4658.
22. Shteynberg D*, et al.* (2011) iProphet: multi-level integrative analysis of shotgun proteomic data improves peptide and protein identification rates and error estimates. *Mol Cell Proteomics* 10(12):M111 007690.
23. Gunjan A & Verreault A (2003) A Rad53 kinase-dependent surveillance mechanism that regulates histone protein levels in S. cerevisiae. *Cell* 115(5):537-549.
24. Lewis PW, Elsaesser SJ, Noh KM, Stadler SC, & Allis CD (2010) Daxx is an H3.3-specific histone chaperone and cooperates with ATRX in replication-

independent chromatin assembly at telomeres. *Proceedings of the National Academy of Sciences of the United States of America* 107(32):14075-14080.
25. Biasini M*, et al.* (2014) SWISS-MODEL: modelling protein tertiary and quaternary structure using evolutionary information. *Nucleic acids research* 42(Web Server issue):W252-258.
26. Arnold K, Bordoli L, Kopp J, & Schwede T (2006) The SWISS-MODEL workspace: a web-based environment for protein structure homology modelling. *Bioinformatics* 22(2):195-201.
27. Bienert S*, et al.* (2017) The SWISS-MODEL Repository-new features and functionality. *Nucleic acids research* 45(D1):D313-D319.
28. Bordoli L*, et al.* (2009) Protein structure homology modeling using SWISS-MODEL workspace. *Nature protocols* 4(1):1-13.
29. Guex N, Peitsch MC, & Schwede T (2009) Automated comparative protein structure modeling with SWISS-MODEL and Swiss-PdbViewer: a historical perspective. *Electrophoresis* 30 Suppl 1:S162-173.
30. Kiefer F, Arnold K, Kunzli M, Bordoli L, & Schwede T (2009) The SWISS-MODEL Repository and associated resources. *Nucleic acids research* 37(Database issue):D387-392.
31. Kopp J & Schwede T (2006) The SWISS-MODEL Repository: new features and functionalities. *Nucleic acids research* 34(Database issue):D315-318.
32. Cao T*, et al.* (2016) Crystal structure of a nuclear actin ternary complex. *Proceedings of the National Academy of Sciences of the United States of America* 113(32):8985-8990.
33. Dokholyan NV, Buldyrev SV, Stanley HE, & Shakhnovich EI (1998) Discrete molecular dynamics studies of the folding of a protein-like model. *Folding & design* 3(6):577-587.
34. Yin S, Ding F, & Dokholyan NV (2007) Eris: an automated estimator of protein stability. *Nature methods* 4(6):466-467.
35. Adzhubei IA*, et al.* (2010) A method and server for predicting damaging missense mutations. *Nature methods* 7(4):248-249.
36. Cheng J, Randall A, & Baldi P (2006) Prediction of protein stability changes for single-site mutations using support vector machines. *Proteins* 62(4):1125-1132.
37. Capriotti E, Fariselli P, & Casadio R (2005) I-Mutant2.0: predicting stability changes upon mutation from the protein sequence or structure. *Nucleic acids research* 33(Web Server issue):W306-310.
38. Lee T & Luo L (1999) Mosaic analysis with a repressible cell marker for studies of gene function in neuronal morphogenesis. *Neuron* 22(3):451-461.
39. Jefferis GS, Marin EC, Stocker RF, & Luo L (2001) Target neuron prespecification in the olfactory map of Drosophila. *Nature* 414(6860):204-208.
40. Stocker RF, Heimbeck G, Gendre N, & de Belle JS (1997) Neuroblast ablation in Drosophila P[GAL4] lines reveals origins of olfactory interneurons. *Journal of neurobiology* 32(5):443-456.
41. Wu JS & Luo L (2006) A protocol for mosaic analysis with a repressible cell marker (MARCM) in Drosophila. *Nature protocols* 1(6):2583-2589.
42. Buenrostro JD, Giresi PG, Zaba LC, Chang HY, & Greenleaf WJ (2013) Transposition of native chromatin for fast and sensitive epigenomic profiling of

open chromatin, DNA-binding proteins and nucleosome position. *Nature methods* 10(12):1213-1218.
43. Bray NL, Pimentel H, Melsted P, & Pachter L (2016) Near-optimal probabilistic RNA-seq quantification. *Nature biotechnology* 34(5):525-527.
44. Love MI, Huber W, & Anders S (2014) Moderated estimation of fold change and dispersion for RNA-seq data with DESeq2. *Genome biology* 15(12):550.
45. Gu Z, Eils R, & Schlesner M (2016) Complex heatmaps reveal patterns and correlations in multidimensional genomic data. *Bioinformatics* 32(18):2847-2849.
46. Chen EY*, et al.* (2013) Enrichr: interactive and collaborative HTML5 gene list enrichment analysis tool. *BMC bioinformatics* 14:128.
47. Kuleshov MV*, et al.* (2016) Enrichr: a comprehensive gene set enrichment analysis web server 2016 update. *Nucleic acids research* 44(W1):W90-97.
48. Langmead B & Salzberg SL (2012) Fast gapped-read alignment with Bowtie 2. *Nature methods* 9(4):357-359.
49. Zhang Y*, et al.* (2008) Model-based analysis of ChIP-Seq (MACS). *Genome biology* 9(9):R137.
50. Quinlan AR & Hall IM (2010) BEDTools: a flexible suite of utilities for comparing genomic features. *Bioinformatics* 26(6):841-842.
51. Yu G, Wang LG, & He QY (2015) ChIPseeker: an R/Bioconductor package for ChIP peak annotation, comparison and visualization. *Bioinformatics* 31(14):2382-2383.
52. Heinz S*, et al.* (2010) Simple combinations of lineage-determining transcription factors prime cis-regulatory elements required for macrophage and B cell identities. *Molecular cell* 38(4):576-589.